formed at the left side of the cavity, together with a weak capillary wave at the right side of the cavity. That only one strong capillary wave is formed at this time instant is the result of the inclination of the surface. The moment at which the rim falls back onto the surface wave is reached earlier at the left side of the cavity, since the distance between the maximum height of the rim and the surface of the liquid pool is smaller. For later time instants the capillary wave trains for the smaller wave move downwards along the surface of the cavity, thereby changing the shape of the cavity downstream of the capillary wave train. Around $t^* = 27.1$ the cavity's shape has changed from hemispherical to elliptical, the capillary waves trains have reached the bottom of the cavity and its retraction motion starts.

For the large surface wave the strong left and weak right capillary waves also start propagating in the direction of the bottom of the cavity for $t^* > 12.3$. Around $t^* = 20.3$ the left capillary wave has reached the position of the surface of the liquid pool at the right side of the cavity. Exactly at this time instant the right side of the rim merges with the surface and a strong capillary wave is formed on this side of the cavity, Figure 5.10(d) and 5.10(h). For larger time instants the receding of the cavity continues symmetrically, until at around $t^* = 30.5$ both capillary waves reach the bottom of the cavity and its retraction begins.

After retraction a Worthington jet is seen to appear for both investigated wave amplitudes. As has been mentioned already before, for the small wave the jet is slightly inclined to the right at the moment it starts to grow in height, which is in correlation with the inclination of the solitary surface wave upon impingement. Just as for the impingement onto $\varphi = 60°$ only a short, thick jet is formed for the large wave, being slightly shifted in the wave propagation direction with respect to the point of impingement. This confirms that for the impingement onto a wave with a large amplitude, a large part of the energy is dissipated during the retraction phase of the cavity.

Overall, it can be stated that a change in the amplification - in amplitude and velocity - of the solitary surface wave changes the impingement process in a pronounced manner for all the investigated phases of the wave at impingement. The time change of the cavity shapes for the impingements onto the small wave is almost identical for both wave-phases; hence the amplitude and velocity of the small solitary surface wave are too small to provoke large differences in the shape of the cavity. Small differences in the position of the capillary waves at the same time instants after impingement are present, leading to small differences in the way the cavity recedes and retracts. This, in turn, results in a central jet which inclination correlates with the inclination of the wave surface.

Large differences are seen between the impingements onto the two different waves for the same wave-phases. A larger wave, hence a larger amplitude and velocity of the surface wave, leads to a corona that interacts strongly with the leading or trailing edge of the wave. For small wave-phases, the cavity expands with a relatively small maximum depth and diameter, whereas for larger phases of the wave the difference of the shape of the cavity for the two waves is smaller. The velocity with which the cavity penetrates into the liquid layer depends strongly on the wave properties.

An earlier and asymmetric receding and retraction of the cavity is seen for the lower wave-phase of the large wave, whereas for the larger wave-phase only minor differences are observed during the receding and retraction phases. The Worthington jet that appears after cavity retraction is thicker and reaches a lower maximum height for the larger waves, partly due to the strong energy dissipation during the retraction and partly due to the weak surface tension forces acting on the small cavity. A thin, high central jet is observed for the small waves, having a slight inclination as a result of the slight asymmetrical receding and retraction of the cavity.

5.1.5 Influence of the liquid properties of the solitary surface wave

It has been shown in §(4.1.4) that the properties of the liquids, hence surface tension and viscosity, have a clear effect on the time evolution of the cavity after impingement. In order to verify how these properties change the cavity expansion, receding and retraction upon impingement onto a solitary surface wave, two different liquids are studied, distilled water and a glycerine/water mixture (30 Vol%/70 Vol%). The properties of these two liquids can be found in Table 3.2.

In this paragraph the evolution of the cavity upon impingement for four investigations are shown in the Figures 5.12 to 5.14 for the non-dimensional times between $t^* = -1.5$ to $t^* = 71.1$. In each of these figures the time change of the shape of the cavities upon impingement onto two phases of the wave ($\varphi \approx 60°$ and $\varphi \approx 147°$) are presented, both for distilled water and glycerine/water. The Weber numbers of the impinging drops remain constant, as well as the amplification and velocity of the wave.

Just as for the discussion of the results for the impingement onto the two different kinds of waves, the analysis of the data presented in this paragraph will be split up into two parts, since the differences between the impingements upon $\varphi \approx 60°$ and upon $\varphi \approx 147°$ are relatively large. First of all the results for $\varphi = 60°$ will be discussed, followed by the discussion of the time change of the cavity for $\varphi = 149°$.

For $\varphi = 60°$ a prompt splash is seen to occur right upon impingement of the drop onto the solitary wave for both liquids. It can be observed that both prompt splashes are more pronounced in the wave propagation direction, because of two phenomena. First of all, the absolute velocity vector is tilted in the direction of the wave propagation, due to the relative velocity of the wave with respect to the drop impingement velocity vector. Second, the right side of the developing corona interacts with the leading edge of the solitary wave, due to which the prompt splash is prohibited at this side.

For larger times after impingement ($t^* \geq 4.4$) the coronas expand in height and diameter, where for distilled water a relatively symmetric expansion is seen. In this case the right side of the corona can expand over the top of the solitary wave, whereas for glycerine/water this right-sided expansion of the cavity is first seen to occur around $t^* = 17.4$. At $t^* = 4.4$ the cavities are seen to expand in radial direction, both in an asymmetrical way with respect to the vertical axis through the point of impingement. For increasing times after impingement it is noted that the inclination of the cavity for the glycerine/water mixture increases more rapidly than for distilled water. This is to be expected, since the viscosity of the glycerine/water mixture is about 2.5 times larger than of distilled water, due to which the top of the cavity propagates stronger with the solitary wave. In combination with the decrease of the film velocity for increasing depth, this leads to a stronger increase of the inclination of the cavity for larger times after impingement, compare Figure 5.12(j) with Figure 5.12(r).

Around $t^* = 17.4$ a strong capillary wave is formed at the right side of the cavity, moving downwards along the surface of the cavity for larger times, thereby changing the shape of the cavity in a pronounced asymmetrical way, Figure 5.13(i). Around $t^* = 30.5$ this capillary wave reaches the bottom of the cavity, at which time the shape of the cavity has changed from hemispherical to conical. In §(4.1.4) it was observed that for higher viscosities of the liquid the capillary waves are formed at a later time instant and their positions and shapes are less pronounced. The same phenomena are observed for the impingement onto a solitary surface wave. For the glycerine/water mixture it is seen that the shape of the cavity changes for $t^* \geq 20.3$, but that the capillary waves, responsible for this change in shape, cannot be observed until around

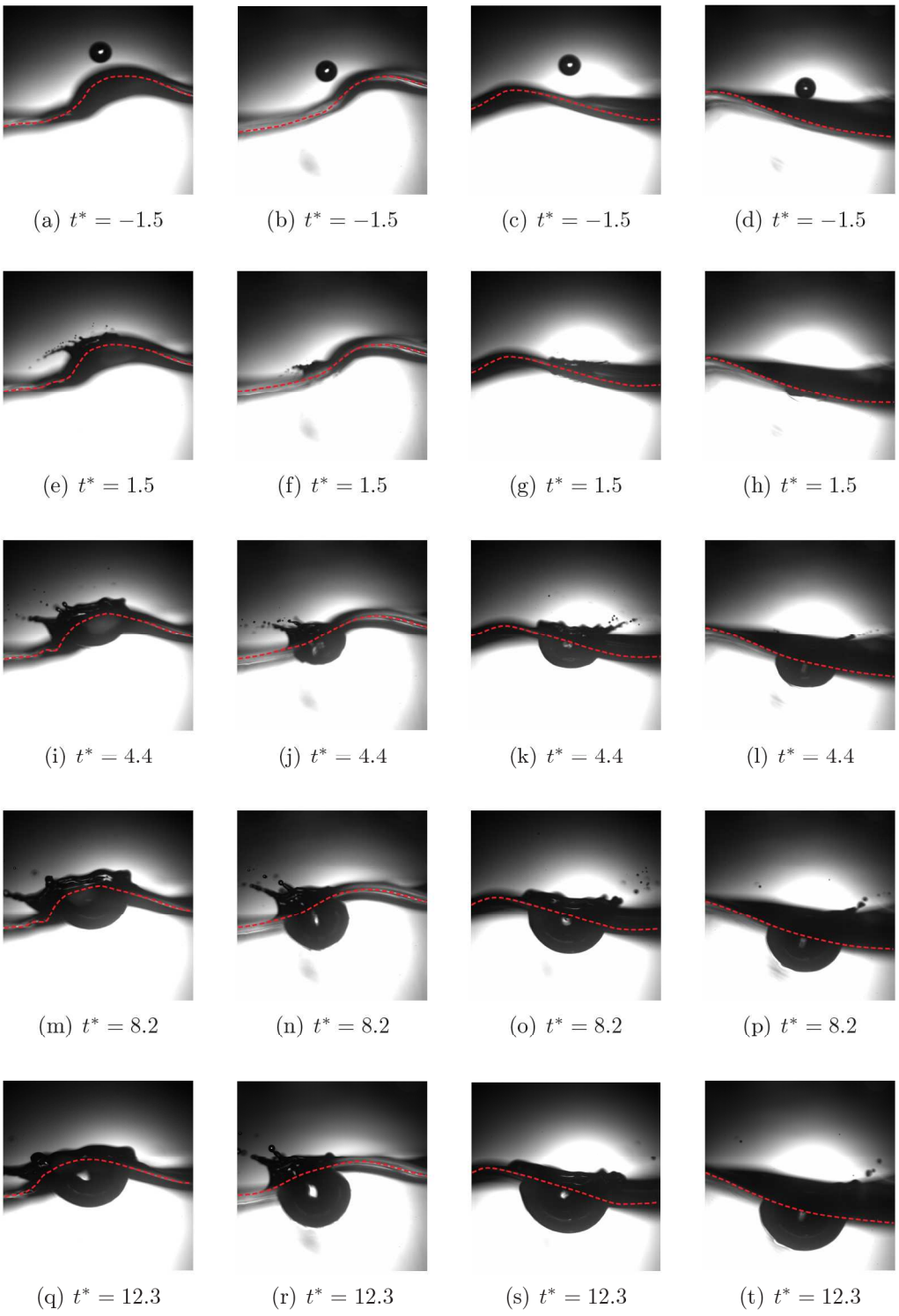

(a) $t^* = -1.5$ (b) $t^* = -1.5$ (c) $t^* = -1.5$ (d) $t^* = -1.5$

(e) $t^* = 1.5$ (f) $t^* = 1.5$ (g) $t^* = 1.5$ (h) $t^* = 1.5$

(i) $t^* = 4.4$ (j) $t^* = 4.4$ (k) $t^* = 4.4$ (l) $t^* = 4.4$

(m) $t^* = 8.2$ (n) $t^* = 8.2$ (o) $t^* = 8.2$ (p) $t^* = 8.2$

(q) $t^* = 12.3$ (r) $t^* = 12.3$ (s) $t^* = 12.3$ (t) $t^* = 12.3$

Figure 5.12: The evolution of the cavity formed by single drop impingement onto a solitary wave at $\varphi = 60°$ and $\varphi = 147°$ for distilled water and a glycerine/water mixture at non-dimensional time instants between $t^* = -1.5$ and $t^* = 12.3$. The impingement parameters are: $U_d = 3.0$ m/s, $D_d = 2.9$ mm and $U_w = 0.4$ m/s (distilled water) and $U_d = 3.0$ m/s, $D_d = 2.6$ mm and $U_w = 0.3$ m/s (glycerine/water). Outer left: $\varphi = 60°$ ($We = 354$, $Fr = 339$, $Re = 10,421$); Middle left: $\varphi = 58°$ ($We = 413$, $Fr = 443$, $Re = 10,944$); Middle right: $\varphi = 147°$ ($We = 342$, $Fr = 348$, $Re = 10,093$); Outer right: $\varphi = 144°$ ($We = 333$, $Fr = 361$, $Re = 9,813$)

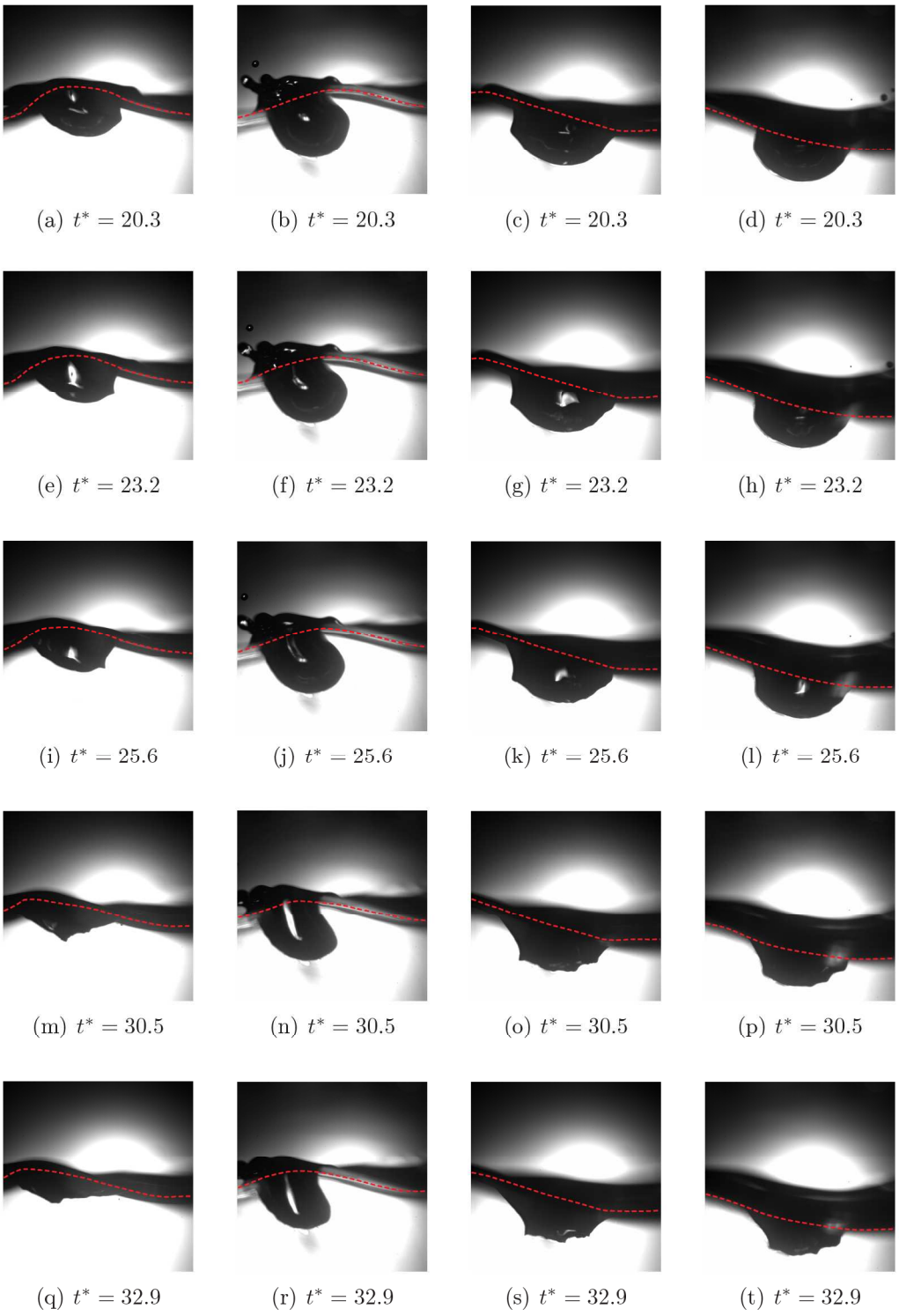

(a) $t^* = 20.3$ (b) $t^* = 20.3$ (c) $t^* = 20.3$ (d) $t^* = 20.3$

(e) $t^* = 23.2$ (f) $t^* = 23.2$ (g) $t^* = 23.2$ (h) $t^* = 23.2$

(i) $t^* = 25.6$ (j) $t^* = 25.6$ (k) $t^* = 25.6$ (l) $t^* = 25.6$

(m) $t^* = 30.5$ (n) $t^* = 30.5$ (o) $t^* = 30.5$ (p) $t^* = 30.5$

(q) $t^* = 32.9$ (r) $t^* = 32.9$ (s) $t^* = 32.9$ (t) $t^* = 32.9$

Figure 5.13: The evolution of the cavity formed by single drop impingement onto a solitary wave at $\varphi = 60°$ and $\varphi = 147°$ for distilled water and a glycerine/water mixture at non-dimensional time instants between $t^* = 20.3$ and $t^* = 32.9$. The impingement parameters are: $U_d = 3.0$ m/s, $D_d = 2.9$ mm and $U_w = 0.4$ m/s (distilled water) and $U_d = 3.0$ m/s, $D_d = 2.6$ mm and $U_w = 0.3$ m/s (glycerine/water). Outer left: $\varphi = 60°$ ($We = 354$, $Fr = 339$, $Re = 10,421$); Middle left: $\varphi = 58°$ ($We = 413$, $Fr = 443$, $Re = 10,944$); Middle right: $\varphi = 147°$ ($We = 342$, $Fr = 348$, $Re = 10,093$); Outer right: $\varphi = 144°$ ($We = 333$, $Fr = 361$, $Re = 9,813$)

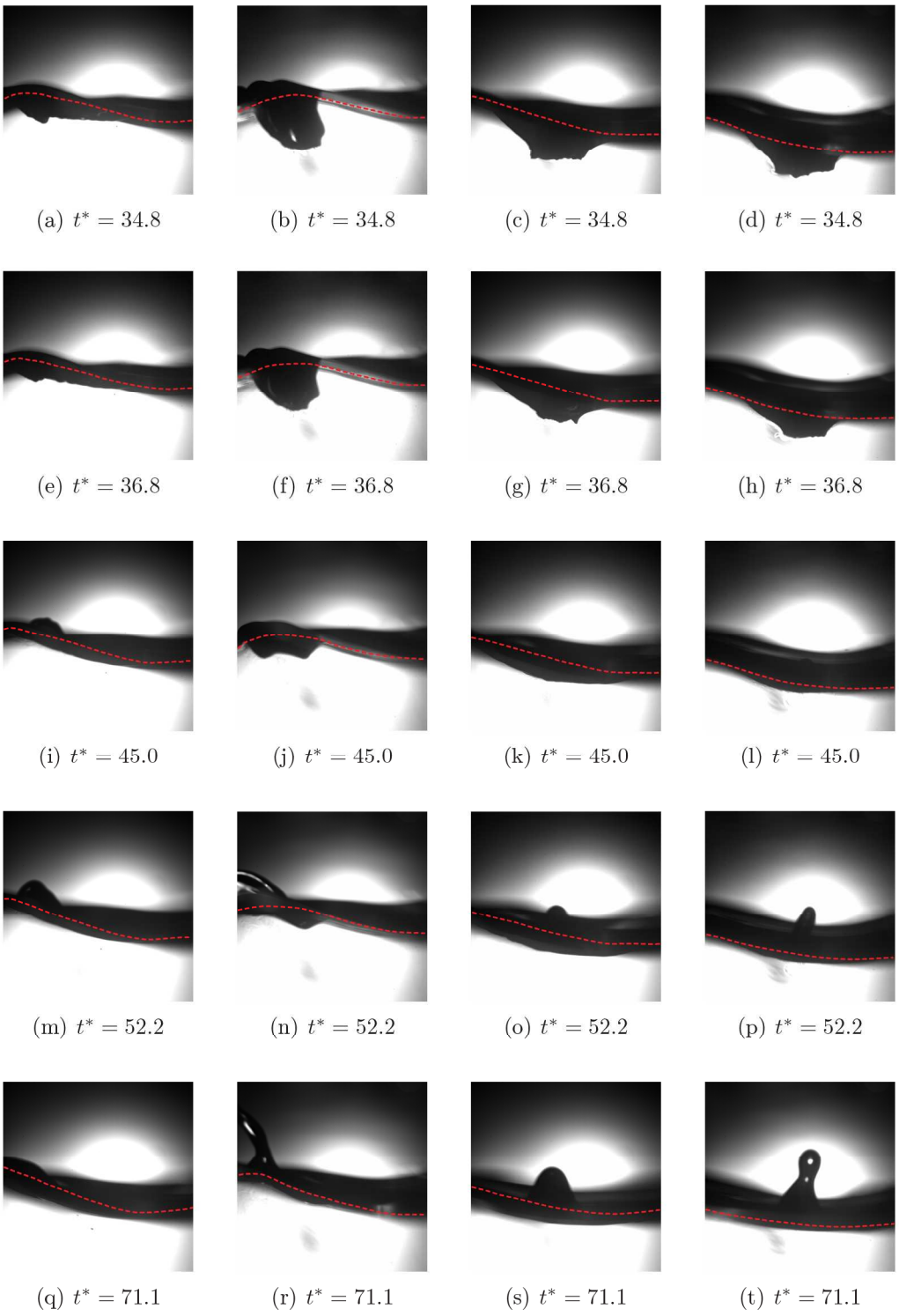

(a) $t^* = 34.8$ (b) $t^* = 34.8$ (c) $t^* = 34.8$ (d) $t^* = 34.8$

(e) $t^* = 36.8$ (f) $t^* = 36.8$ (g) $t^* = 36.8$ (h) $t^* = 36.8$

(i) $t^* = 45.0$ (j) $t^* = 45.0$ (k) $t^* = 45.0$ (l) $t^* = 45.0$

(m) $t^* = 52.2$ (n) $t^* = 52.2$ (o) $t^* = 52.2$ (p) $t^* = 52.2$

(q) $t^* = 71.1$ (r) $t^* = 71.1$ (s) $t^* = 71.1$ (t) $t^* = 71.1$

Figure 5.14: The evolution of the cavity formed by single drop impingement onto a solitary wave at $\varphi = 60°$ and $\varphi = 147°$ for distilled water and a glycerine/water mixture at non-dimensional time instants between $t^* = 34.8$ and $t^* = 71.1$. The impingement parameters are: $U_d = 3.0$ m/s, $D_d = 2.9$ mm and $U_w = 0.4$ m/s (distilled water) and $U_d = 3.1$ m/s, $D_d = 2.6$ mm and $U_w = 0.3$ m/s (glycerine/water). Outer left: $\varphi = 60°$ ($We = 354$, $Fr = 339$, $Re = 10,421$); Middle left: $\varphi = 58°$ ($We = 413$, $Fr = 443$, $Re = 10,944$); Middle right: $\varphi = 147°$ ($We = 342$, $Fr = 348$, $Re = 10,093$); Outer right: $\varphi = 144°$ ($We = 333$, $Fr = 361$, $Re = 9,813$)

$t^* = 34.8$. At this moment a strong capillary wave appears at the right side of the cavity, together with a small capillary wave at the left side, which have reached already approximately the bottom of the cavity at this time. Due to the differences in strength of both capillary waves the cavity recedes asymmetrically, where the shape of the cavity at the right side is changed more pronounced by the stronger capillary wave.

This asymmetrical receding results in an additional increase of the inclination of the cavity during the receding phase. The subsequent contraction of the cavity, starting around $t^* = 40.7$, is therefore also asymmetrically, thereby forming a W-shape of the cavity for glycerine/water (Figure 5.14(j)), leading to a thin jet, being curved over approximately 90° at its formation, Figure 5.14(n). In Figure 5.14(r) is can be seen that for larger times the Worthington jet starts to erect itself. For distilled water, however, only a short, thick jet is formed after retraction of the cavity, Figure 5.14(m), due to the small values of the surface tension forces acting on the cavity, leading to smaller values of the kinetic energy available for the formation of the Worthington jet. Both jets are shifted in the wave propagation direction, as a result of the drifting of the cavities during their expansions, the asymmetries of the motions and strengths of the capillary waves and the subsequent asymmetrical receding of the cavities.

The recordings of the impingements onto the wave-phase $\varphi \approx 147°$ for distilled water and for glycerine/water show no distinct differences. Right after impingement, at $t^* = 1.5$, a prompt splash is observed for both liquids, leading to the generation of the secondary droplets. For $t^* = 4.4$ it is seen that for both liquids the coronas can expand freely to the right, whereas the left side of the coronas interact with the trailing edges of the solitary surface waves. The cavities expand for both liquids in a highly symmetrical way, until around $t^* = 12.3$ the rims, having fallen back onto the liquid surfaces due to gravity, merge with these liquid surfaces and generate a strong capillary wave at the left side of the cavities. At the right side of the cavities, a weak capillary wave is formed, although its existence cannot be observed until $t^* = 30.5$.

These capillary waves move downwards along the surface of the cavities, thereby changing the cavity's shapes downstream of the capillary waves. At the moment that the strong left capillary waves reach approximately the same vertical level as the liquid surface at the right side of the cavities, a strong capillary wave at the right side is formed, Figure 5.13(g) (distilled water) and Figure 5.13(l) (glycerine/water). It is noted that these time instants are respectively $t^* = 23.2$ for distilled water and $t^* = 25.6$ for glycerine/water. The capillary waves at the left side of the cavities penetrate the liquid pools for both liquids with approximately the same propagation velocity. Due to the different times at which the capillary waves are formed at the right side of the cavities, a symmetrical receding of the cavity is found for distilled water, whereas for the glycerine/water mixture the right capillary wave lacks behind the left capillary wave. The latter results in an earlier deformation of the shape of the cavity from convex to concave at the left side of the cavity, Figure 5.13(t).

Around $t^* = 34.8$ the capillary waves at both sides of the cavity reach the bottom of the cavity for both investigated liquids, which is followed by a merging of the capillary waves to the center of the cavity. This merging of the capillary waves is combined simultaneously with a retraction of the cavity, resulting from the surface tension forces acting on the cavity. Due to the upward motion of the cavity a Worthington jet is formed for both investigated liquids, being thick and short for distilled water and thin and long for the glycerine/water mixture. In comparison to the impingements onto a wave-phase of $\varphi \approx 60°$ the central jets for $\varphi \approx 147°$ are formed relatively close to the horizontal point of drop impingement.

Looking at the different impingement outcomes for distilled water and glycerine/water,

it can be stated that a change in the properties of the liquid - surface tension and viscosity - of the solitary surface wave has a distinct influence on the outcome of the impingement process for low values of the phase of the wave at impingement. For relatively large wave-phases only minor differences are observed during the expansion, receding and retraction phases of the cavity.

Large differences are seen between both liquids for the impingements onto small wave-phases. A smaller value of the viscosity leads to a cavity that expands less in radial direction, resulting in a smaller maximum depth and diameter. For increasing times after impingement the inclination of the cavity for the glycerine/water mixture increases more rapidly than for distilled water, resulting from a stronger propagation of the top of the cavity in the direction of wave propagation, in combination with the decrease of the film velocity for increasing depth.

An earlier and asymmetric receding and retraction of the cavity is seen for distilled water, which, in combination with the weak surface tension forces, leads to a thick, short Worthington jet. As a result of the pronounced asymmetrical receding and retraction of the cavity for glycerine/water the Worthington jet that appears for this liquid, is highly curved at formation, erecting itself for later time instants.

5.2 Penetration, expansion, receding and retraction of the cavity

This paragraph presents the detailed quantitative results of the diameter and depth evolution of the cavity in time upon impingement of a single drop onto a wavy liquid surface. Two different surface wave topologies have been investigated, the standing wave and the solitary surface wave. For the first class of waves, the standing waves, the amplitude of the wave, being for the studies presented hereafter a function of time only, and the phase of the wave upon impingement influence the impingement outcomes, whereas for the solitary surface waves, the impingement results are directly influenced by the amplitude, phase and velocity of the wave, as well as by the velocity distribution inside the surface film. By comparing the results for these two kinds of surface waves, not only the influence of the inclined film surface on the drop impingement will become clear, but also the velocity distribution of the surface film, introducing a relative velocity component upon impingement and a continuous motion of the film during the cavity evolution. These results set a major step in the direction of the realistic modeling of spray impingement, where the motion of the surface film plays a significant role.

Several particular impingements of the many impingement experiments conducted are selected and presented in more detail hereafter. The impingement parameters of all the conducted experiments and numerical simulations are listed in Table 5.2.

5.2.1 Evolution of the cavity in time upon impingement onto a standing wave

To study the influence of the inclination of the liquid surface film on the cavity behaviour in time, fully three-dimensional numerical simulations of the single drop impingement onto a wavy liquid surface are conducted. For the simulations presented hereafter, a standing wave without continuous added energy is simulated. This means that at the start of the simulation a surface wave is initiated, which levels-off in time due to the influence of surface tension and gravity

Table 5.2: Parameters of the conducted experiments and numerical simulations used for the discussion of the impingement outcomes of the single drop impingement upon standing waves and solitary surface waves

Liquid	**Amplified**	h^*	We	Fr	Re	$Phase$	$D^*_{cav,max50\%}$	$t^*_{cav,max50\%}$	$D^*_{cav,max75\%}$	$t^*_{cav,max75\%}$	$Depth^*_{max}$	$t^*_{depth,max}$
Isopropanol	Standing	2.0	189	127	1,199	180°	2.85	9.6	-	-	1.88	17.3
Isopropanol	Standing	2.0	527	366	1,982	180°	4.09	22.4	-	-	1.92	32.6
Isopropanol	Steady	2.0	189	127	1,199	-	2.97	10.8	-	-	1.99	16.9
Isopropanol	Steady	2.0	527	366	1,982	-	4.15	21.5	-	-	1.94	43.1
Distilled water	No	5.8	304	251	10,411	26°-146°	2.96-3.13	10.6-12.9	2.38-2.56	10.7-12.4	1.80-2.34	11.9-13.4
Distilled water	No	5.8	378	269	11,611	21°-134°	3.20-3.47	13.2-15.5	2.55-2.84	13.2-15.0	1.89-2.45	14.0-15.1
Distilled water	No	5.8	398	328	11,458	31°-162°	2.59-3.51	14.6-17.9	2.09-2.80	15.1-17.6	1.81-2.27	15.6-18.0
Distilled water	Yes	5.8	285	296	9,170	31°-178°	2.73-4.47	15.1-22.5	2.09-3.62	15.0-21.9	1.15-2.61	15.0-22.7
Distilled water	Yes	5.8	346	351	10,169	24°-179°	2.02-4.49	14.7-25.5	1.56-3.47	15.1-25.7	0.61-2.86	15.7-23.0
Distilled water	Yes	5.8	389	391	10,796	24°-163°	2.78-4.74	17.2-25.8	2.19-3.90	15.5-27.6	1.26-3.22	17.4-26.9
Glycerine/water	No	6.4	185	203	7,276	14°-138°	3.26-3.72	11.3-13.4	2.60-3.09	13.1-14.8	1.94-2.18	14.6-15.7
Glycerine/water	No	6.4	232	252	8,191	7°-126°	3.66-3.97	13.6-15.6	2.89-3.13	16.5-18.5	2.18-2.38	13.6-15.6
Glycerine/water	No	6.4	284	316	8,980	-1.5°-122°	3.77-4.14	18.0-20.2	2.84-3.08	16.0-20.8	2.18-2.43	15.4-19.8
Glycerine/water	Yes	6.4	282	310	9,004	15°-166°	3.37-4.20	16.8-21.8	2.41-3.17	15.1-22.4	1.36-2.64	16.6-21.9
Glycerine/water	Yes	6.4	337	364	9,873	36°-153°	3.48-4.70	16.9-23.8	2.67-3.49	16.8-24.1	1.68-3.19	17.0-22.5
Glycerine/water	Yes	6.4	361	407	10,112	12°-166°	3.34-4.77	16.7-27.9	2.64-3.67	18.0-25.1	1.63-3.00	18.0-23.6
Distilled water	Steady	5.8	296	302	9,397	-	4.09	20.4	3.23	18.6	2.61	18.8
Distilled water	Steady	5.8	309	218	10,520	-	3.13	11.5	2.56	11.2	2.34	12.9
Distilled water	Steady	5.8	353	388	10,063	-	4.46	22.5	3.47	21.0	2.86	19.4
Distilled water	Steady	5.8	381	406	10,539	-	4.59	25.8	3.71	23.4	2.61	20.2
Distilled water	Steady	5.8	382	269	11,703	-	3.45	14.4	2.84	14.2	2.49	14.0
Glycerine/water	Steady	6.4	189	201	7,418	-	3.43	11.3	2.79	14.0	2.11	14.9
Glycerine/water	Steady	6.4	237	251	8,322	-	3.67	13.6	2.90	16.9	2.27	14.5
Glycerine/water	Steady	6.4	275	306	8,846	-	3.77	18.4	2.86	16.0	2.25	15.4
Glycerine/water	Steady	6.4	339	367	9,883	-	4.29	21.9	3.49	20.3	2.50	18.5
Glycerine/water	Steady	6.4	362	416	10,072	-	4.59	25.0	3.67	20.4	2.79	21.8

into a steady liquid film of thickness h. This leveling process, however, takes much longer than the drop impingement process itself, as will be presented below, due to which the wavy liquid surface still influences the cavity below the liquid surface at the end of the impingement process. The initial shape of the liquid surface can be described by:

$$y_{film}(t, \mathbf{x}) = Acos(k\mathbf{x} - \varphi) + h \tag{5.1}$$

Here is A the wave amplitude, $k = 2\pi/\lambda$ the wave number, λ the wavelength, $\mathbf{x}$ the position coordinate in space, φ is the phase of the wave at which the drop impinges, t the time and h the initial mean dimensional film thickness. The value of the phase of the wave at impingement and the initial liquid film thickness are set to $\varphi = 180°$ and $h^* = 2.0$ respectively, resulting in the amplitude of the wave being a function of time only. This wave phase is chosen, because the largest influence of the curved liquid surface on the impingement outcomes is to be expected. Furthermore, a non-dimensional wave amplitude of $A^* = A/D_d = 0.46$ and a non-dimensional wavelength of $\lambda^* = \lambda/D_d = 7.15$ are set.

Evolution of shape of the cavity in time

In Figure 5.15 and Figure 5.16 the numerical results of the evolution of the cavity's shape at different non-dimensional time instants after impingement upon a standing wave are shown for isopropanol. In these images the solid lines represent the boundaries between the gas phase and the liquid phase, the vertical dashed line is the symmetry axis going through the center of the impinging drop. The impingement parameters are $We = 189$, $Fr = 127$ and $Re = 1,199$ for the first figure and $We = 527$, $Fr = 366$ and $Re = 1,982$ for the second figure. For both impingement studies, the liquid film height and phase of the wave at impingement are set to $h^* = 2.0$ and $\varphi = 180°$ respectively.

When comparing the time change of the corona and the cavity between the impingement onto steady liquid films (Figure 4.7 and 4.8 for $We = 527$ and $Re = 1,982$) and standing waves several distinct differences can be observed. Right upon impingement a clear difference in the formation of the corona is observed for both Weber numbers. At the left side of the cavity, where the instantaneous film thickness upon impingement is higher, a thicker rim is formed at a higher vertical position seen from the bottom of the liquid, Figures 5.15(b) and 5.16(b). The shape of the rim at the right side of the cavity develops in time in the same way as is observed for the impingement onto a steady liquid film. The higher value of the kinetic energy of the impinging drop for $We = 527$ leads in the next time instants to a distinct formation and expansion of the corona, which even becomes unstable at the right side of the cavity. This results in a secondary droplet formation at this side of the cavity, whereas at the left side the corona remains stable. For the simulated case with a lower Weber number, Figure 5.15, the corona is seen to expand in time, but no instabilities are observed, as the kinetic energy of the drop is not high enough to initiate these instabilities.

The formation and expansion phase of the cavity are seen to occur in an asymmetrical manner. For both impingement Weber numbers the cavity at the right side of the symmetry axis expands faster in diameter. This is the direct result of the difference in the film height at both sides of the symmetry axis, being smaller at the right. Due to this smaller film height and the symmetrical penetration of the cavity in vertical direction into the liquid film, the surface of the cavity at the right side is smaller than at the left side. This leads to smaller surface tension forces acting on the cavity and opposing its expansion, due to which the cavity can expand more in radial direction, see for example Figure 5.15(d) and 5.16(d).

The height of the corona at the left side of the cavity is smaller than at the right side, which

leads to an earlier non-dimensional time instant at which the left side of the corona falls back onto the liquid film and merges with this film.

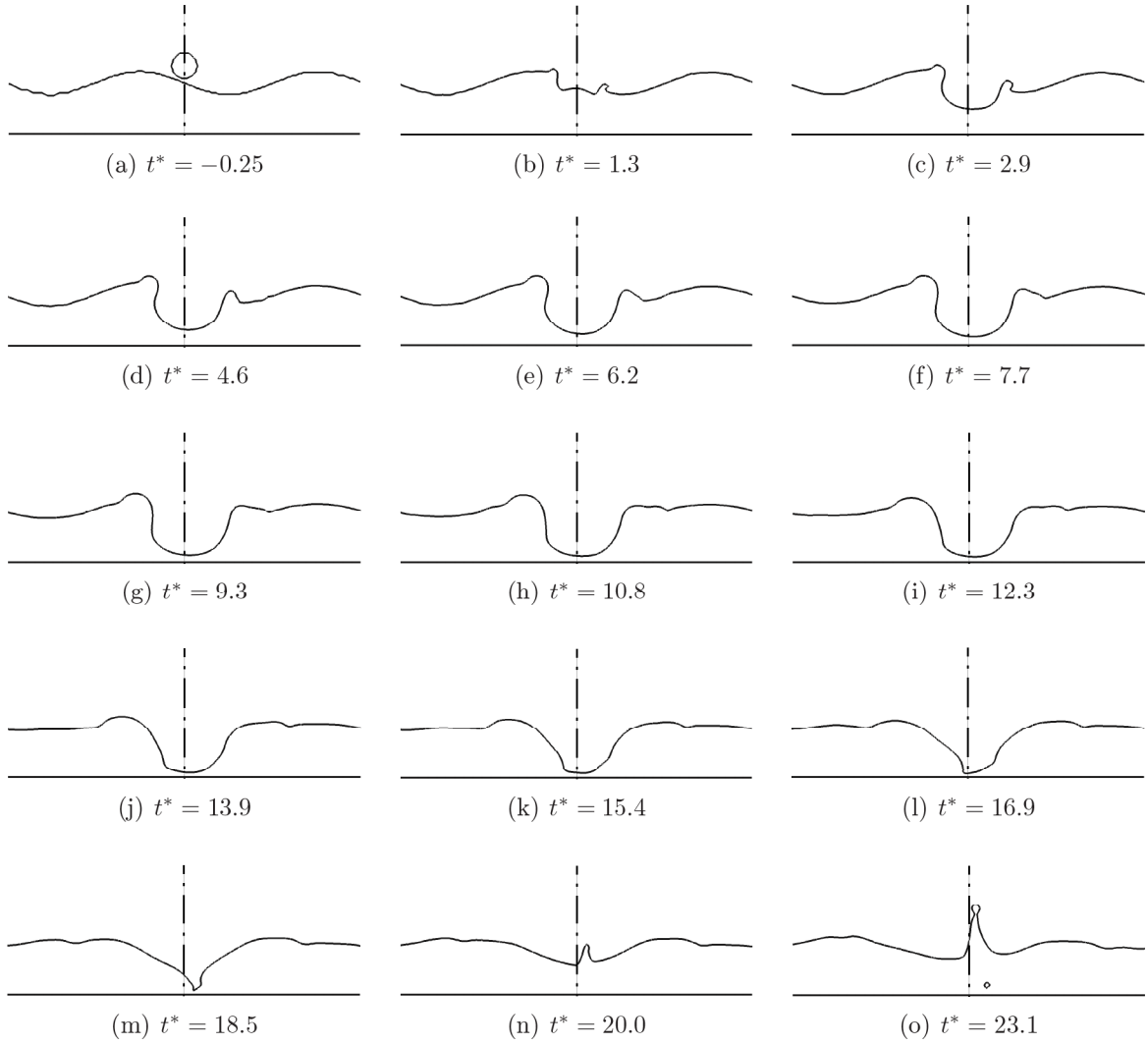

Figure 5.15: Numerical simulations of the single drop impingement onto a standing wave. The evolution of the cavity formed by an isopropanol drop impingement at non-dimensional time instants between $t^* = -0.25$ and $t^* = 23.1$ The impingement parameters are $D_d = 2.1$ mm, $U_d = 1.6$ m/s, $A^* = 0.46$, λ^* 7.15 and $\varphi = 180°$ ($We = 189$, $Fr = 127$, $Re = 1,199$)

At this time instant, hence $t^* = 4.6$ and $t^* \approx 19$ for respectively $We = 189$ and $We = 527$, a capillary wave is formed at the inside of the left side of the cavity due to a sudden pressure increase upon merging of the rim with the liquid film. In the following time instants the left capillary wave moves downwards along the surface of the cavity, thereby changing the shape of the cavity downstream of the wave. In Figure 5.16(f) it is observed that the right capillary wave is formed around the same time instant as the left capillary wave, but at a higher vertical position inside the rim. This lag in vertical position between both capillary waves at the same time instant leads to a clear asymmetrical receding of the cavity, where the left side of the cavity changes earlier from hemispherical into a conical shape. The same behaviour is observed

for $We = 189$, for which the capillary wave at the right is formed around $t^* = 12.3$. At this time instant the left capillary wave has reached already approximately the bottom of the cavity, hence the cavity's left shape has changed at this moment already from hemispherical to conical, whereas the right side of the cavity is about to start changing in shape.

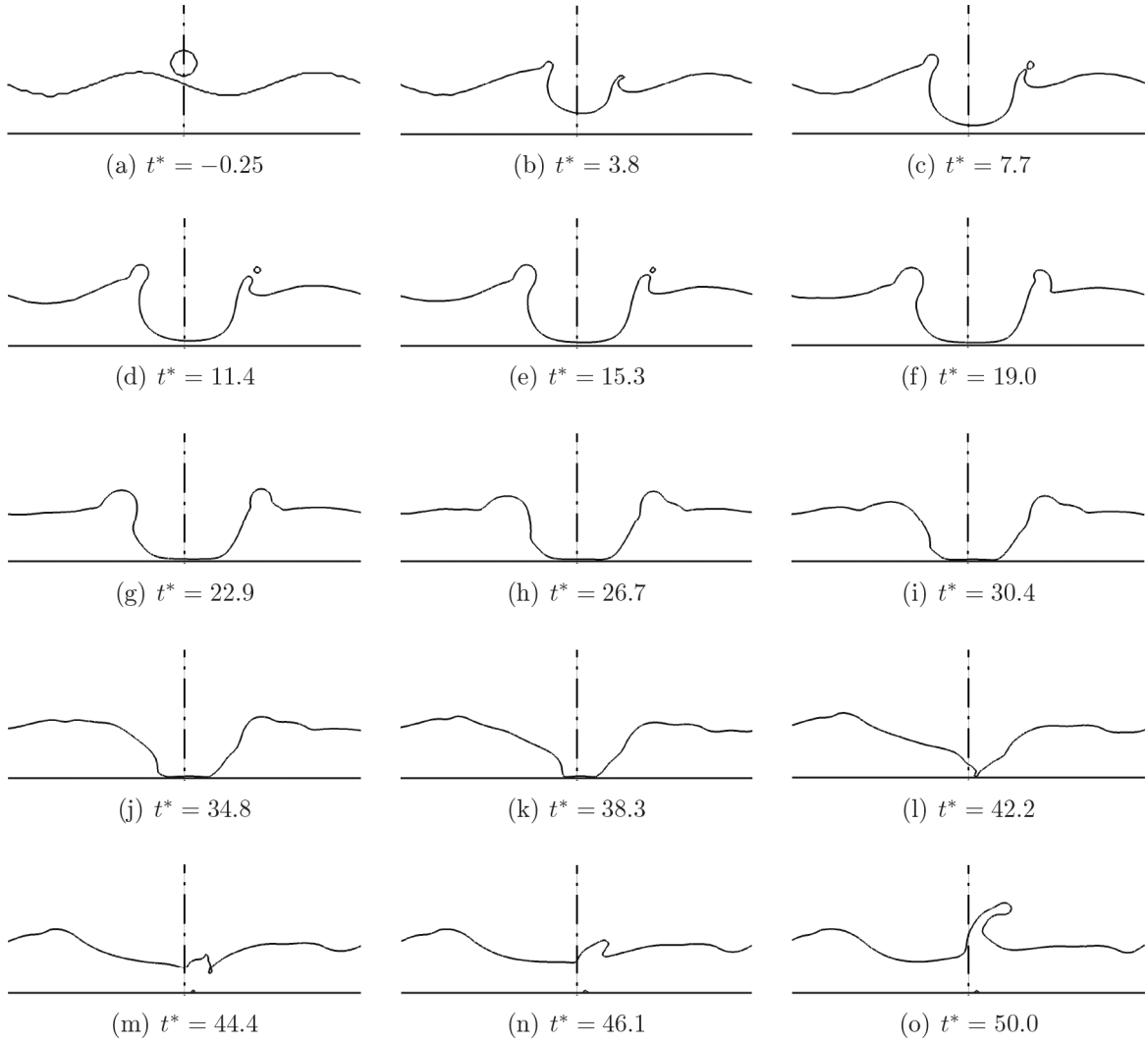

Figure 5.16: Numerical simulations of the single drop impingement onto a standing wave. The evolution of the cavity formed by an isopropanol drop impingement at non-dimensional time instants between $t^* = -0.25$ and $t^* = 50.0$ The impingement parameters are $D_d = 2.1$ mm, $U_d = 3.1$ m/s, $A^* = 0.46$, λ^* 7.15 and $\varphi = 180°$ ($We = 527$, $Fr = 366$, $Re = 1,982$)

At respectively $t^* = 13.9$ and $t^* = 34.8$ for $We = 189$ and $We = 527$ the left capillary wave reaches the bottom of the cavity and starts its translating motion along the bottom of the cavity to the cavity's center. Since for both investigated impingements the right capillary wave lags the left capillary wave in position, an asymmetrical contraction of the bottom of the cavity is seen for both Weber numbers. For the lower Weber number, this lag in position between both capillary waves is so large, that before the right capillary wave has reached the bottom of the cavity, which is around $t^* = 18.5$, the left capillary wave has crossed the central

axis from the left to the right, Figure 5.15(m). At the moment the cavity starts its retracting motion, the cavity shape looks like a cone that is inclined to the left. Due to this inclination and the position of the capillary waves just before retraction, a slight inclined Worthington jet is formed. The position of this jet is not central, as is the case for impingements upon steady liquid films, but has drifted slightly to the right with respect to the central axis, as a result of the position of both capillary waves at retraction.

The receding phase of the cavity for the higher investigated Weber number occurs in a different way. At $t^* = 34.8$ the left capillary wave reaches the bottom of the cavity and starts its motion to the center. Due to the penetration of the capillary wave at the right side of the cavity and the surface tension forces acting on the cavity, the shape of the cavity is changed from hemispherical to conical as well. Around $t^* = 42.2$ the left capillary wave has crossed the central axis and a sharp cone angle is formed at the bottom of the cavity. At this moment the right capillary wave has reached a vertical position that equals approximately half of the depth of the cavity. As a result of the strong pressure forces acting on the bottom of the cavity and the asymmetrical receding, the cavity starts to retract in a highly asymmetrical way. At $t^* = 44.4$ two important phenomena are observed. First of all it is seen that the initial Worthington jet is inclined to the right. Second, at exactly this moment it is observed at the right side of the image that the retracting cavity and the Worthington jet interact with the right capillary wave. Exactly this interaction leads to an inflection of the inclination of the jet. This can be seen clearly in Figure 5.16(o), where the initial part of the Worthington jet, hence in this image the upper part of the jet, is inclined to the right, and the lower part of the jet is inclined to the left.

Evolution of the depth and diameter of the cavity in time

By comparing the time evolution of the cavities, formed after impingement onto a steady liquid film and onto a standing wave, several distinct differences in the shapes of the cavities are noticed. In order to investigate whether the topology of the liquid surface film has also a clear effect on the typical length and time scales of the cavities, the time change of the depth of the cavity, hence its lowest point, and of the diameter of the cavity at half its maximum depth have been studied in detail.

The time changes of the depths of the cavities for the impingements of isopropanol drops onto steady liquid films and onto standing waves are presented in Figure 5.17. The liquid film thickness is $h^* = 2.0$, the impingement parameters of the drops are listed in Table 5.2 together with the maximum depths of the cavities and the non-dimensional times at which these depths are reached.

This figure clearly shows that the penetration velocity of the cavity, which equals $U^*_{cav} = 0.5$ for the impingement upon steady liquid films, is not influenced by the inclination of the surface film. This has two main consequences. First of all, the inclination of the surface film has no influence at all on the time evolution of the cavity during the expansion phase. Second, the curves of the impingements onto standing waves show during the expansion phase of the cavities for both simulated Weber numbers exactly the same behaviour. This is in conformity with the results of the impingements onto steady liquid films, shown in Chapter 4, where it was found that the depth evolution of the cavity during the expansion phase is independent on the Weber number of the impinging drop.

Close to the time instant at which the cavities start to retract, two distinct differences are observed between both investigated surface film topologies. The time instant at which the

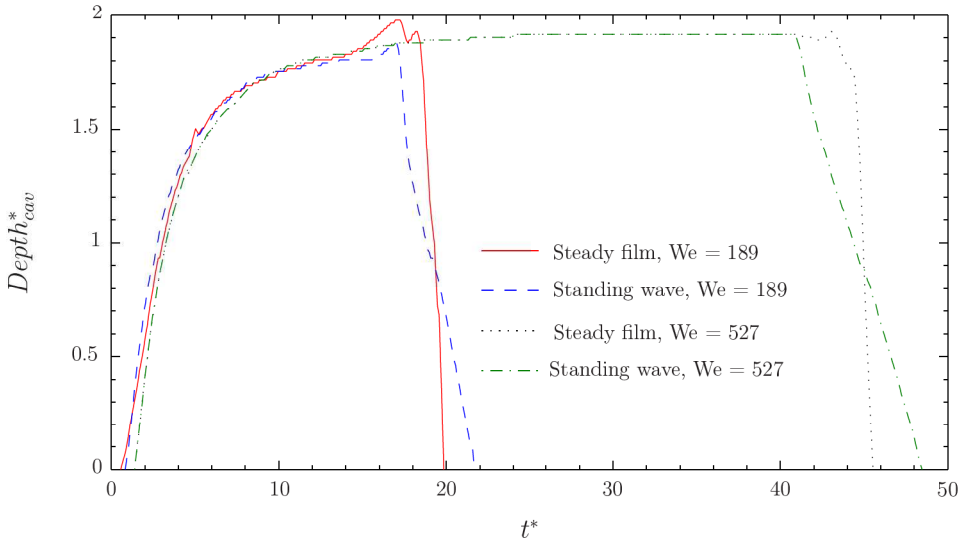

Figure 5.17: Evolution of the depth of the cavity in time upon a single drop impingement for isopropanol. Comparison of the numerical simulations for the impingement onto a steady liquid surface film and onto a standing wave for $We = 189$ and $We = 527$ ($h^* = 2.0$)

cavity starts to retract is found to occur earlier for the impingement onto a standing wave and the velocity with which the cavity retracts is smaller. Both phenomena can be explained by looking at the images in the Figures 5.15 and 5.16. In these images it was observed that the capillary wave at the left side of the cavity is formed earlier and reaches therefore the bottom of the cavity at an earlier time instant. This leads for both Weber numbers to an asymmetrical receding of the cavity and merging of the capillary waves. The result is a sooner change of the bottom of the cavity from hemispherical to conical and therefore the high pressure forces, responsible for the retraction of the cavity, act earlier on the cavity than is the case for the impingement onto a steady liquid film. Because the capillary wave at the right side has not reached the bottom yet at the moment the cavity starts its retracting motion, the angle of the cone is blunter, which leads to a lower value of these high pressure forces. This results in a lower retraction velocity, as is observed in Figure 5.17 for both Weber numbers.

The second important length scale for single drop and spray impingement is the time evolution of the diameter of the cavity at half its maximum depth, D^*_{cav}. The results of the numerical simulations for the diameter evolution of the impingements onto steady liquid films and onto standing waves are presented in Figure 5.18 for $We = 189$ and in Figure 5.19 for $We = 527$. In both figures the diameter changes of the impingements upon standing waves are split up into three parts: the absolute, hence total, diameter, and the relative diameter at the left and at the right side of the vertical axis going through the center of the drop at impingement. The last two relative diameters give an indication of the symmetry of the cavity: in case of a completely symmetrical cavity, these two values will be the same and equal to half the total diameter.

When comparing the curves of the total diameter of the cavity for the impingement onto a standing wave for both Weber numbers (the dotted lines in both figures), the same observations can be made as for the impingement onto a steady liquid film, Chapter 4. An impingement with a larger Weber number of the drop leads to a wider cavity, since more kinetic energy

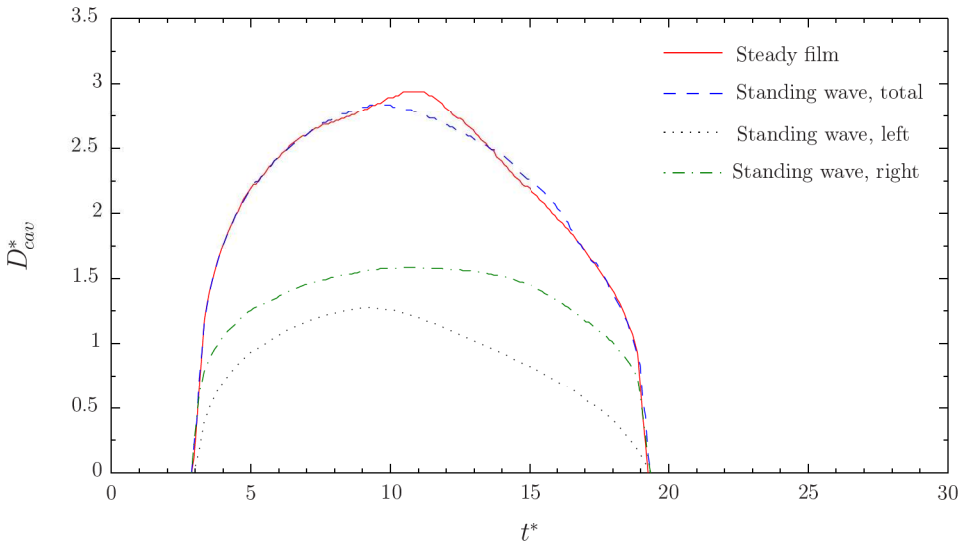

Figure 5.18: Evolution of the diameter of the cavity in time upon a single drop impingement for isopropanol. Comparison of the numerical simulations for the impingement onto a steady liquid surface film and onto a standing wave (total, left side and right side) for $We = 189$ and $h^* = 2.0$

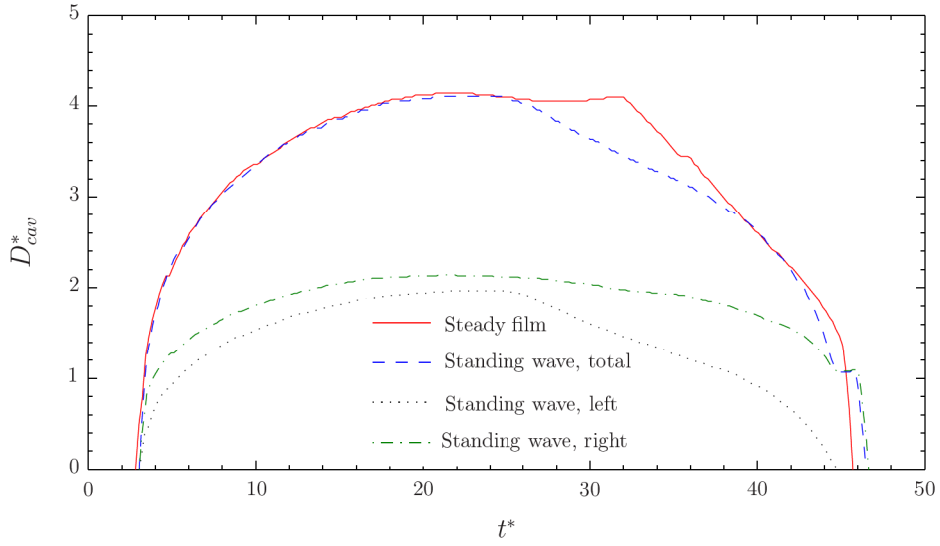

Figure 5.19: Evolution of the diameter of the cavity in time upon a single drop impingement for isopropanol. Comparison of the numerical simulations for the impingement onto a steady liquid surface film and onto a standing wave (total, left side and right side) for $We = 527$ and $h^* = 2.0$

is available upon impingement to overcome the surface tension forces. This leads to a larger maximum value of the cavity diameter and a later non-dimensional time instant at which this maximum diameter is reached, of which the values are given in Table 5.2. Due to the later time instant at which the surface tension forces can overcome the kinetic energy and the wider cavity, the receding of the cavity starts later and takes longer, resulting in a later time instant at which the curve equals zero, compare $t^* \approx 19$ for $We = 189$ with $t^* \approx 46$ for $We = 527$.

A direct comparison between the curves of the total diameter of the cavity for both surface topologies shows that the inclination of the surface has little to no effect on the radial expansion of the cavity. The difference in surface film topology, however, has a clear influence on the cavity diameter during the receding phase. For the impingement onto steady liquid films the maximum value of the diameter is reached at the moment at which both capillary waves pass the vertical point at which the time evolution of the diameter is measured, hence $y^*_{cav}/Depth^*_{cav,max} = 0.5$. In the Figures 5.15 and 5.16 it was shown that an inclined surface upon impingement results in a difference in time at which the capillary waves at the left and at the right side of the cavity are formed. This means that the capillary waves pass the point $y^*_{cav}/Depth^*_{cav,max} = 0.5$ one after another, resulting in a lower value of the maximum diameter, as can be seen for both Weber numbers in Figure 5.18 and 5.19. Additionally, for $We = 527$ the earlier formation of the capillary wave at the left side of the cavity leads to an earlier receding of the cavity, thereby enhancing the decrease of the total diameter.

The asymmetry in the diameter of the cavity with respect to the vertical axis through the center of the impinging drop is clearly visible for both Weber numbers. The values of the diameter at the left side of the cavity (the dotted line in both figures) are smaller during the completely impingement process, being the result of two different phenomena.

First of all, the slope of the film surface at impingement is for both investigated Weber numbers declining, meaning that the drop "sees" at impingement a higher film thickness at its left than at its right. During the expansion phase the cavity is seen to expand in depth with a constant velocity, independent of the inclination and Weber number, due to which the surface of the cavity is larger at its left side. This results in larger values of the surface tension forces at this side, acting on the cavity and trying to oppose the further expansion of the cavity. Due to these higher surface tension forces, the kinetic energy is converted sooner, therefore leading to lower values of the cavity diameter than at the right side of the cavity. For lower Weber numbers the difference between the cavity diameter at the left and right side is larger, as the direct result of the lower available kinetic energy upon impingement.

During the receding phase the differences between the values of the diameter at both sides of the cavity are the direct result of the capillary waves. Due to the lower rim at the left side of the cavity and the subsequent earlier merging of the rim with the liquid surface, the capillary wave is formed earlier at this side. Form the moment this capillary wave starts moving downwards the shape of the cavity at this side is changed from hemispherical to conical, hence the diameter is decreased. At the right side of the cavity the later formation and downward motion of the capillary wave results in a later decrease of the diameter at this side, thereby introducing large differences between the diameters at both sides.

It can therefore be concluded that the inclination of the liquid surface film upon impingement has a very distinct influence on the time evolution of the shape of the cavity and the typical length and time scales. For a descending wave, where the left side of the wave, seen from the center of the drop, is higher than the right side, the rim is thicker at the left side. At this side the rim remains stable, whereas at the right side, a corona can be formed, which can become unstable in case of a high impingement Weber number, leading to droplet formation.

The penetration of the cavity in depth direction is independent of the inclination angle of the liquid surface and the Weber number, whereas a clear influence of the inclination is observed for the radial expansion. At the left side of the cavity the surface film is higher, due to which the surface of the cavity is larger at this side. This results in larger values of the surface tension forces at this side, leading to a faster conversion of the kinetic energy. Although the time evolution of the total diameter of the cavity is not influenced by the inclination angle, the inclination of the standing wave leads to lower values of the cavity diameter at the left side of the cavity. This difference between the diameters of the cavity at both sides becomes larger for lower Weber numbers.

Due to the lower rim at the left side of the cavity and the subsequent earlier merging of the rim with the liquid surface, the capillary wave is formed earlier at this side. During the receding and retraction phase, this time difference in capillary wave formation at both sides of the cavity introduces several clear differences between the cavities formed after impingement upon the two investigated liquid surface film topologies. Summarised the main differences are a lower value of the maximum diameter of the cavity, an asymmetrical downward motion of the capillary waves and receding of the cavity, thereby introducing large differences between the values of the local diameters at both sides of the cavity, an asymmetrical merging of the capillary waves and an off-axis Worthington jet of which its inclination and curvature increase with increasing Weber number.

5.2.2 Time change of the cavity upon impingement onto a solitary surface wave

The numerical simulations of the single drop impingement onto the wave-phase of 180° of a standing wave, described in the paragraph above, have shown that the inclination of the liquid surface film, hence the local difference in film thickness, has a very distinct influence on the evolution of the shape of the cavity in time. For spray impingement, however, not only the inclination of the surface film plays a significant role on the outcome of the impingement process, but also the velocity distribution and fluctuations of the surface film itself. These velocity fluctuations are introduced by the simultaneous and/or subsequent neighbouring impingements of the drops of the spray.

To follow one impinging drop of the spray, in order to study the influence of the fluctuations of the surface film on its impingement during spray impingement, is close to impossible. In this thesis, the first significant experimental step in understanding the complete spray impingement process is made. Here, the spray impingement process is simulated by a single drop impingement onto a moving solitary wave. In this way, not only the inclination of the film surface is taken into account, but also the velocity distribution inside the film itself.

In the first paragraph of this chapter the observations of the single drop impingements onto solitary waves have been described in detail with the use of Shadowgraph images. For this study, the Weber number of the impinging drop, the phase of the wave at impingement, the amplification (velocity and maximum amplitude) of the solitary surface wave and the liquid properties were changed, to investigate their influences on the impingement outcomes.

In this section the complete evolution of the depth and the diameter, the latter one measured at $y_{cav}/Depth^*_{cav,max} = 0.5$, of the cavity with time will be presented and discussed. The discussion is split up into two parts: first the evolution of the depth of the cavity is presented and analysed, followed by the evolution of the diameter of the cavity in time. In each of the two paragraphs the influences of the parameters mentioned above are investigated and explained.

From all the experimental data - 740 measurements with different settings - only a selected group is shown in this section.

Time evolution of the depth of the cavity

In Chapter 4 it was shown that the single drop impingement process onto steady liquid surface films is very repeatable. For the time evolution of the depth of the cavity and the diameter of the cavity, measured at half its maximum depth, the repeatability lies around 98.5 %. To assure that the results of the single drop impingements onto solitary surface waves can be trusted both qualitatively as well as quantitatively, each measurement is repeated five times, after which its deviation from the mean is calculated.

The time evolutions of the depths of the cavities upon several phases of the solitary surface wave for the five repeated measurements are shown in Figure 5.20 for the small wave and in Figure 5.21 for the large amplified surface wave. In each of the figures the results for all three investigated Weber numbers are presented.

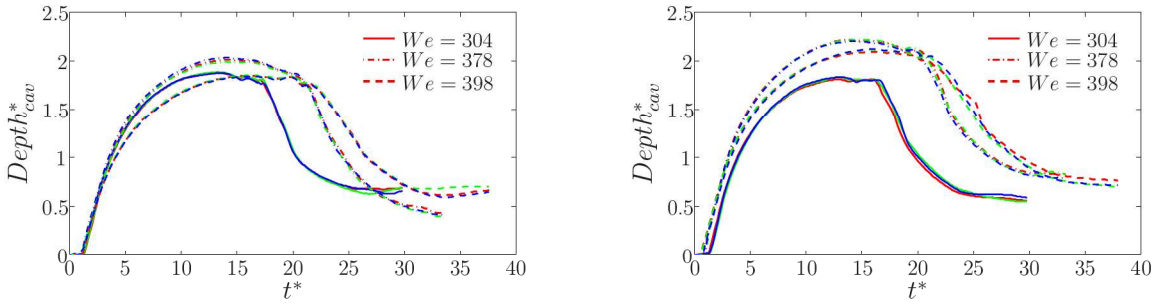

(a) Distilled water, $\varphi = 59°$

(b) Distilled water, $\varphi = 148°$

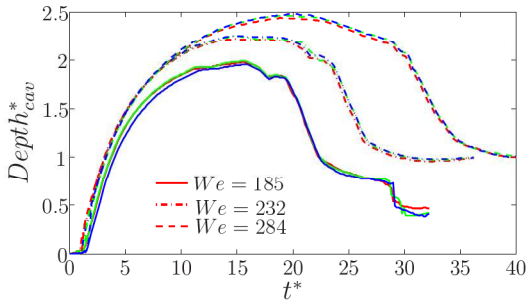

(c) Glycerine/water, $\varphi = 69°$

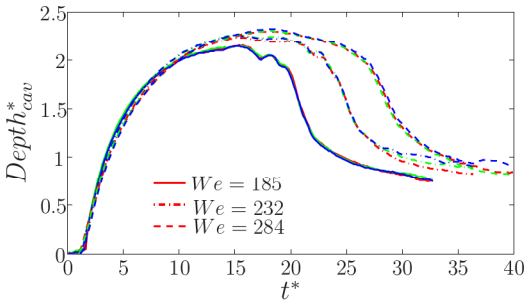

(d) Glycerine/water, $\varphi = 145°$

Figure 5.20: Repeatability study for the single drop impingement onto different phases of the small amplified wave for distilled water and glycerine/water. The impingement parameters are listed in Table 3.2 and 5.2

Both figures show that for these measurements the three curves lie very close together. This means not only that there exists a very high repeatability of the single drop impingement process upon both solitary waves, but also that the amplification of the waves, hence their velocity and amplitude, are approximately equal for each measurement. The mean spreading of the depth evolution in time is presented in Table 5.3 for the measurements shown in Figure 5.20 and 5.21. It is observed that for the depth evolution the spreading lies always below 5%.

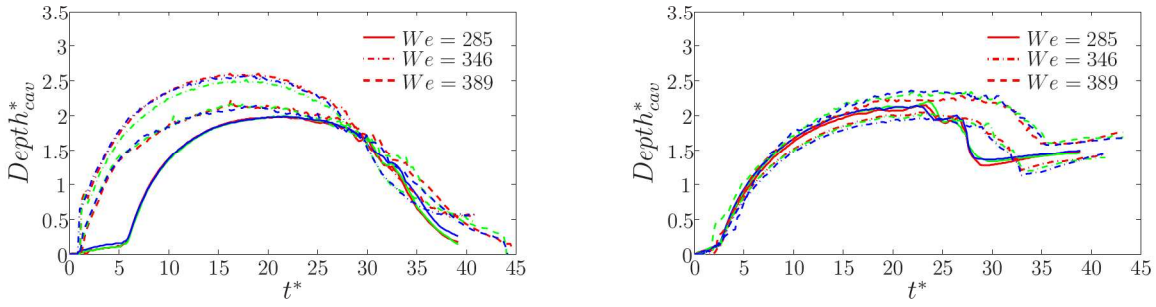

(a) Distilled water, $\varphi = 20°$

(b) Distilled water, $\varphi = 127°$

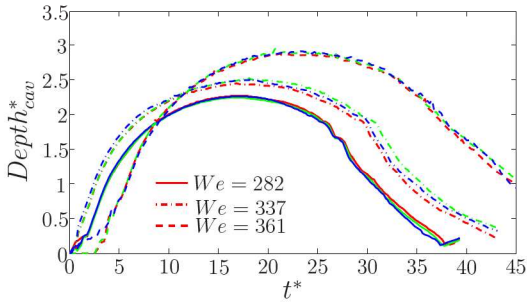

(c) Glycerine/water, $\varphi = 26°$

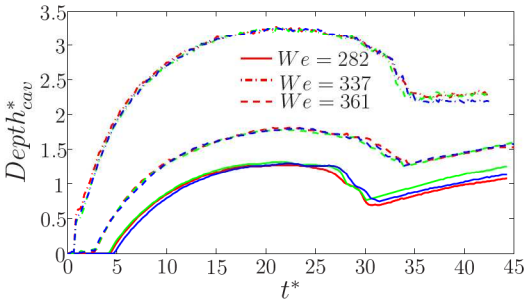

(d) Glycerine/water, $\varphi = 102°$

Figure 5.21: Repeatability study for the single drop impingement onto different phases of the large amplified wave for distilled water and glycerine/water. The impingement parameters are listed in Table 3.2 and 5.2

This low spreading between the different measurements justifies that for the discussion of the results of the time evolution of the depth for different parameters, presented hereafter, the mean depth evolution is taken over the five repeated measurements. This is done, in order to avoid a misinterpretation of the results in case of possible larger spreading between the repeated measurements.

Plots of the non-dimensional cavity depth ($Depth^*_{cav}$) against the non-dimensional time (t^*) upon different phases of the solitary surface waves are given in Figure 5.22 for the small amplified wave and in Figure 5.23 for the large amplified wave. In each figure the results for two of the three investigated absolute Weber numbers, hence based on the combined velocity of the impinging drop and the solitary surface wave, are presented for both investigated liquids. As a reference, for each case the time evolution of the depth for the impingement upon a steady liquid surface film of equal thickness is shown as well.

When looking at the time evolution of the depth of the cavity for the impingement upon small amplified waves (Figure 5.22) it is observed that right upon impingement the penetration of the cavity in depth is constant for all presented wave-phases. Their slopes are equal to the slope of the curve for the impingement upon a steady liquid film, meaning that the penetration velocity of the cavity is independent of the phase of the wave upon impingement.

For distilled water the curves for all investigated wave-phases lie below the reference curve for the impingement upon a steady liquid film. At larger times after impingement the cavity expands radially into the liquid film, thereby increasing its surface. This leads to an increase

Table 5.3: Mean spreading of the results for the depths and absolute diameters of the cavities after five repeated measurements

Liquid	**Amplification**	φ [°]	**We** [-]	**Fr** [-]	**Re** [-]	**Standard deviation in depth [%]**	**diameter [%]**
Distilled water	Small	59	304	215	10,411	1.6	3.6
Distilled water	Small	59	378	269	11,611	2.5	4.5
Distilled water	Small	59	398	328	11,458	1.9	3.6
Distilled water	Small	148	304	215	10,411	2.8	4.1
Distilled water	Small	148	378	269	11,611	2.2	4.6
Distilled water	Small	148	398	328	11,458	3.3	5.1
Distilled water	Large	20	285	296	9,170	2.8	3.3
Distilled water	Large	20	346	351	10,169	4.0	4.3
Distilled water	Large	20	389	391	10,796	4.7	2.0
Distilled water	Large	127	285	296	9,170	3.2	4.7
Distilled water	Large	127	346	351	10,169	4.0	2.8
Distilled water	Large	127	389	391	10,796	4.1	6.1
Glycerine/water	Small	69	185	203	7,276	3.0	4.0
Glycerine/water	Small	69	232	252	8,191	2.0	4.5
Glycerine/water	Small	69	284	316	8,980	2.0	3.4
Glycerine/water	Small	145	185	203	7,276	1.2	4.4
Glycerine/water	Small	145	232	252	8,191	3.7	3.6
Glycerine/water	Small	145	284	316	8,980	2.1	4.7
Glycerine/water	Large	26	282	310	9,004	2.51	4.5
Glycerine/water	Large	26	337	364	9,873	6.12	5.4
Glycerine/water	Large	26	361	407	10,112	3.68	4.5
Glycerine/water	Large	102	282	310	9,004	4.78	4.9
Glycerine/water	Large	102	337	364	9,873	3.47	5.9
Glycerine/water	Large	102	361	407	10,112	1.91	3.9

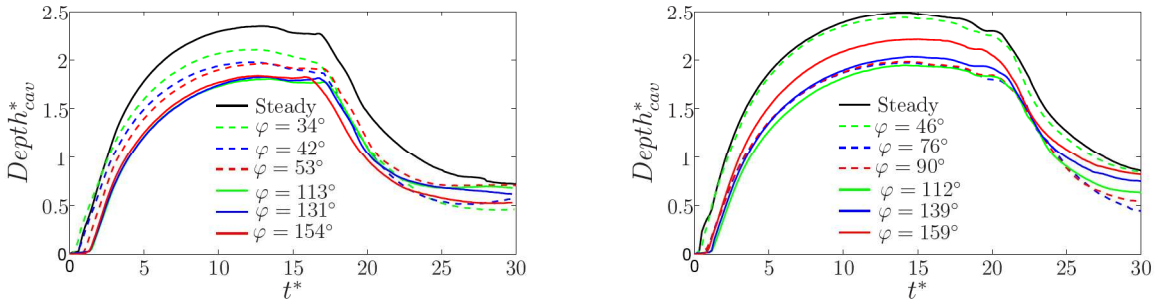

(a) Distilled water, $We = 304$, $Re = 10,411$

(b) Distilled water, $We = 378$, $Re = 11,611$

(c) Glycerine/water, $We = 185$, $Re = 7,276$

(d) Glycerine/water, $We = 232$, $Re = 8,191$

Figure 5.22: Evolution of the depth of the cavity in time as a function of the phase of the wave upon impingement onto the small amplified wave. Comparison of the experimental results for different Weber numbers and liquids. The impingement parameters are listed in Table 3.2 and 5.2

of the surface tension forces, opposing the further expansion of the cavity, due to which the rate of expansion of the cavity becomes smaller for larger times; hence the curves describing the depth evolution in time start to level off. The leveling of these curves, however, depends strongly on the phase of the wave at impingement. For an impingement upon the leading edge of the solitary wave, hence within the range of wave-phases $0° \leq \varphi \leq 90°$, a larger inclination of the wave surface, i.e. a higher value of the wave-phase, leads to a faster leveling of the curve. For larger film surface inclinations the film surface at the right side of the cavity is higher. This results in a clear interaction of the right side of the rim with the surface film, due to which a lower rim is formed at this side. Due to the earlier influence of gravity, the merging of the rim takes place sooner, leading to an earlier formation of the capillary wave at the right side of the cavity. Due to the presence of this capillary wave, the receding of the cavity is initated, leading to an earlier leveling of the curve for the depth evolution in time.

The impingements upon the trailing edge of the solitary wave, hence within the range of wave-phases $90° \leq \varphi \leq 180°$, show a completely different behaviour. For the lowest investigated Weber number no influence of the wave-phase is observed for the depth evolution of the cavity during its expansion phase, whereas for the higher Weber number an increase in wave-phase leads to a later leveling of the curves. For the higher Weber number more kinetic energy is available upon impingement. In combination with the lower inclination of the surface film for higher wave-phases, hence a less interaction of the rim with the surface wave, this leads to a lower rate of energy conversion during the expanding phases and a later formation of the

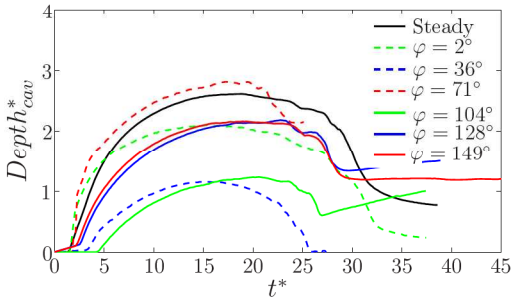

(a) Distilled water, $We = 285$, $Re = 9,170$

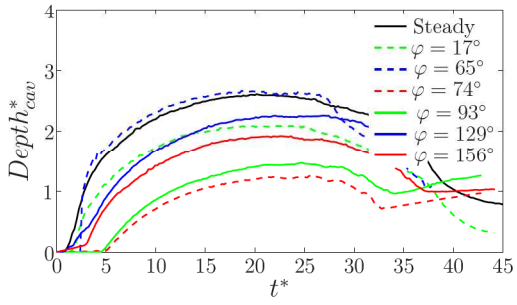

(b) Distilled water, $We = 389$, $Re = 10,796$

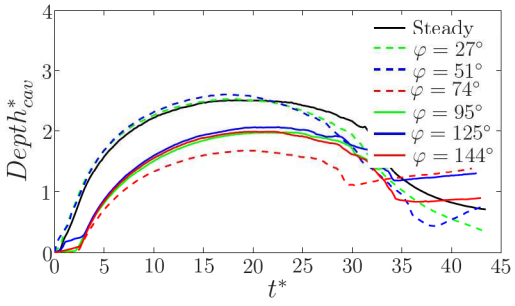

(c) Glycerine/water, $We = 337$, $Re = 9,873$

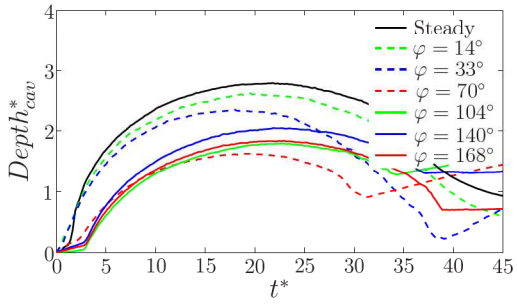

(d) Glycerine/water, $We = 361$, $Re = 10,112$

Figure 5.23: Evolution of the depth of the cavity in time as a function of the phase of the wave upon impingement onto the large amplified wave. Comparison of the experimental results for different Weber numbers and liquids. The impingement parameters are listed in Table 3.2 and 5.2

capillary waves, therefore a later leveling of the curves.

For the glycerine/water mixture the differences in the curves of the depth evolution of the cavity for different wave-phases, as observed for distilled water, are not so distinct. Most curves lie close to the curve which describes the time evolution of the depth for the impingement upon a steady liquid film. This is the result of the higher viscosity of the fluid, leading to a smaller velocity and maximum amplitude of the solitary wave and therefore a smaller inclination of the surface film. Due to this relatively small wave velocity, the solitary wave has no direct influence on the cavity, hence the differences between the impingement upon a solitary wave and upon a steady liquid film are small.

After the complete conversion of the kinetic energy into surface tension energy and dissipated energy the maximum depth of the cavity is reached. Since the thickness of the liquid pool is $h^* = 5.8$ for distilled water and $h^* = 6.4$ for glycerine/water, no interaction of the cavity with the bottom of the liquid pool is observed. The values of the maximum depth and the time at which these maximum depths are reached are presented at the left side of Figure 5.24 and 5.25 respectively, for all investigated Weber numbers and liquids.

These figures clearly show that although the differences between the curves for different Weber numbers, liquids and wave-phases upon impingement are large, the values of the maximum depth and of the time at which these maximum depths are reached are near to constant. A slight increase of both parameters is seen for larger phases of the wave, but these differences

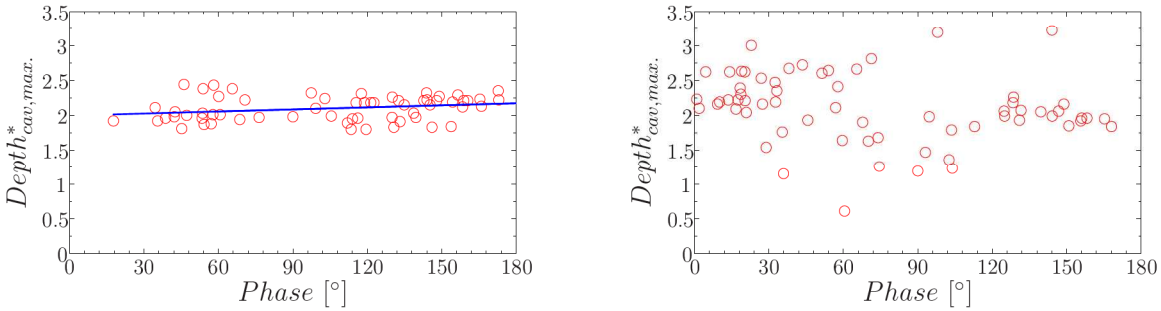

(a) Small wave (b) Large wave

Figure 5.24: Maximum depth of cavity as a function of the phase of the wave upon impingement for both wave amplifications

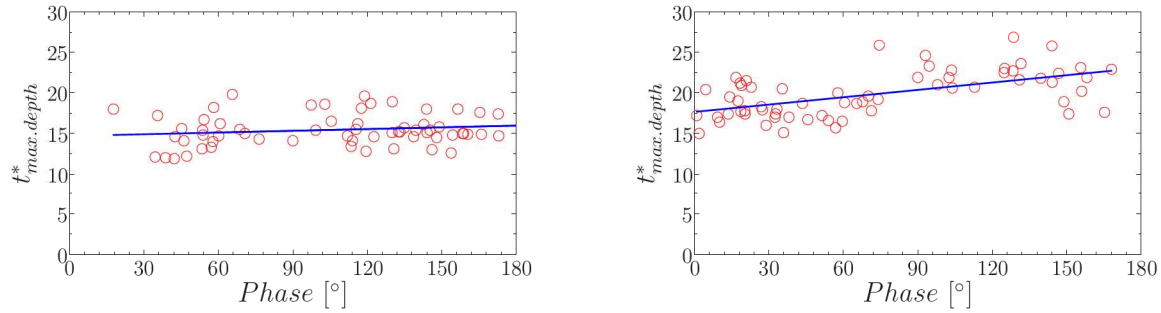

(a) Small wave (b) Large wave

Figure 5.25: Time to reach maximum depth of cavity as a function of the phase of the wave upon impingement for both wave amplifications

are only minor. It can therefore be concluded that for the impingement upon a small amplified solitary wave the overall influence of the investigated parameters on the maximum depth and time of maximum depth is negligible.

After the maximum depths have been reached, the receding and subsequent retraction of the cavity is initiated. The results, presented in Figure 5.22, show only minor differences in the retraction of the cavities for the investigated wave-phases. A later retraction of the cavities is observed for both liquids for higher Weber numbers, which is in agreement with the observations of the impingements upon steady liquid films for different Weber numbers. Due to the larger value of the kinetic energy for larger Weber numbers, a wider cavity is formed together with a higher rim, resulting in a later formation of the capillary waves and a larger time-span during which the cavity recedes, hence a later retraction of the cavity.

The time evolutions of the depths of the cavities upon impingement onto a large amplified wave are presented in Figure 5.23. For both distilled water and glycerine/water large differences are seen between the curves for different wave-phases and different Weber numbers.

The slopes of the curves during the increasing phase of the cavities depend strongly on the phase of the wave upon impingement. For distilled water the slopes for the impingements upon the leading edge of the solitary wave show no clear dependency on the phase of the wave, whereas for the impingements upon the trailing edge of the solitary wave an increase in the

slope with increasing wave-phase is observed for all investigated Weber numbers. Due to the weaker interaction of the rim with the surface of the wave upon impingement onto the trailing edge of the wave the penetration of the cavity into the liquid film is less influenced by the solitary surface wave.

For glycerine/water, however, it is seen that the slopes of the curves for the impingements onto the leading edge of the wave decrease for increasing wave-phases. This decrease of the slopes becomes faster the more the phase of the wave upon impingement approaches $\varphi = 90°$. The explanation for this decrease in the slope of the curves is the following. It is observed that for wave-phases close to $\varphi = 90°$ the rim can expand freely at both sides of the cavity, without interacting at the right side with the leading edge of the solitary wave. Due to the absence of the interaction with the solitary wave, this rim does not become unstable. The top of the left side of the cavity moves with approximately the same velocity as the wave, whereas the right side can expand less due to the opposing motion of the liquid and the increasing surface tension forces. This leads to a cavity, which is elongated horizontally, but not vertically. Due to the earlier merging of the capillary wave at the right side of the cavity, this leads to an earlier receding of the cavity. For the low wave-phases the curves lie close to the curve for the impingement upon a steady liquid film, since for these phases the cavity gets more inclined for later times. Due to the expansion of the cavity in radial direction, the lowest point of the cavity changes position, it moves along the bottom of the cavity from the right to the left. This effect cancels out the stronger inclination of the cavity in time; hence, when looking at the curve of the depth evolution, it looks like the cavity expands in depth in a normal way. This is in contrast to the observations, made for distilled water, where also for very low wave-phases already a very distinct influence of the solitary wave can be seen, compare for example the curve for $\varphi = 2°$ in Figure 5.23(a) with the curve for $\varphi = 27°$ in Figure 5.23(c). This is the result of the velocity of the solitary wave, which is larger for distilled water, thereby leading to a larger horizontal component of the absolute velocity vector. This means that already at low wave-phases less kinetic energy is available to overcome the surface tension forces during the expansion of the cavity. In combination with the formation of the capillary wave at the left side of the cavity at only a few non-dimensional time instants upon impingement, this leads to a fast leveling of the curve for the depth of the cavity in time. The time evolution of the depth for the impingements onto the trailing edge of the solitary surface wave are for glycerine/water nearly constant for different wave-phases, whereas for distilled water it is seen that an increase in the wave-phase between $90° \leq \varphi \leq 180°$ leads to an increase in the slope of the curves.

After the complete conversion of the kinetic energy into surface tension energy and dissipated energy the maximum depth of the cavity is reached. The values of the maximum depth and the times at which these maximum depths are reached are presented as a function of the phase of the wave at the right side of Figure 5.24 and 5.25 respectively for all investigated Weber numbers and liquids. No clear dependency is observed between the values of the maximum depth and the wave of the phase upon impingement. It is noted that around $\varphi = 90°$ the values are approximately twice as small in comparison with the other phases, which has also been observed in §(5.1) and in Figure 5.22 and 5.23. The explanation can be found in the local shape of the solitary wave at impingement, the formation and shape of the rim and the influence of the propagation of the solitary surface wave on the radial expansion of the cavity, as has been explained in detail above. Larger values of the time at which the maximum depth is reached are found for increasing wave-phases, Figure 5.25(b). This is explained by the interaction of the rim with the solitary surface wave, the way the capillary waves are formed, their downward motion and subsequent receding of the cavity, see Chapter §(5.1).

After the maximum depths have been reached, the receding and subsequent retraction of

the cavity is initiated. The results presented in Figure 5.23 show that large differences in the retraction of the cavities are also present for the investigated wave-phases. A later retraction of the cavities is observed for both liquids for higher Weber numbers, which is in agreement with the observations of the impingements upon steady liquid films and smaller amplified waves for different Weber numbers, due to the larger value of the kinetic energy upon impingement in combination with the relatively weak influence of the solitary surface wave.

The second parameter, varied to study its influence on the impingement outcomes, is the absolute Weber number of the impinging drop. For each liquid, wave-phase and amplification the depth evolution of the cavity in time for three different Weber numbers has been investigated. For two of these three Weber numbers the results are presented below. Figure 5.26 shows the time evolution of the depth of the cavity upon impingement onto the small amplified wave; the results for the large amplified wave are presented in Figure 5.27. In each of these figures, Subfigure (a) and (b) show an overview of the results for respectively distilled water and glycerine/water. These subfigures present the depth evolutions in time for several of the investigated phases of the wave, together with the reference cases, hence the impingements upon a steady liquid surface film. In each of the Subfigures (c) to (f) the results for one single phase of the wave are shown, to highlight clearly the influences of the Weber number on the results. Because of the large differences between the results of the two wave topologies, the discussion will be split up into two parts: the results for the impingement onto the small solitary wave, followed by those for the large surface wave.

For both investigated liquids the velocity with which the cavities penetrate into the liquid film is constant for the small amplified wave, which is stated once more by the constant slopes of the time evolutions of the depths for all investigated wave-phases. For distilled water it is observed that for lower Weber numbers of the impinging drop, the curves start to level-off earlier. Because of the lower kinetic energy available upon impingement for lower Weber numbers, this kinetic energy can be overcome earlier by the surface tension energy, leading to a smaller expansion of the cavity. It has to be noted that for distilled water the curves for all investigated wave-phases lie below the reference curve for the impingement upon a steady liquid film, Figure 5.26(a). This is the result of the motion of the liquid film, leading to a slightly wider cavity with a lower depth. Together with the slightly asymmetric merging of the rim and the subsequent time-shifted formation of the capillary waves at both sides of the cavity, this leads to a faster conversion of the kinetic energy than is the case for the impingement onto a steady liquid film.

For the glycerine/water mixture the Weber number of the impinging drop has little to no influence on the time evolution of the depth for the expansion phase of the cavity. With the exception of the curve for $\varphi = 69°$, all curves presented in Figure 5.26(b) follow the same trend during the expansion phase of the cavity. A slightly earlier leveling of the curves is seen for lower Weber numbers, although the differences are small in comparison to the results for distilled water. For $\varphi = 69°$ a larger influence of the lowest Weber number is seen, due to the relatively steep inclination of the surface at this phase angle, in comparison to the other investigated phases. For this specific wave angle this results in a stronger interaction of the rim of the cavity with the leading edge of the solitary wave, leading to a slightly stronger asymmetrical formation of the capillary waves at both sides. In combination with the relatively low value of the kinetic energy upon impingement for this Weber number, this results in a faster conversion of the kinetic energy, hence an earlier leveling of the curve for the depth evolution of the cavity, Figure 5.26(d).

The values of the maximum depth and the times at which these maximum depths are

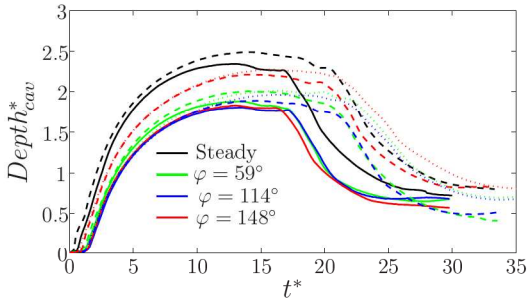

(a) Distilled water, small wave

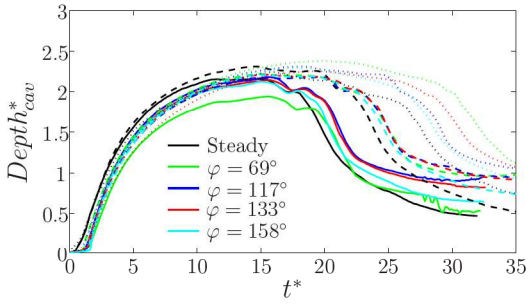

(b) Glycerine/water, small wave

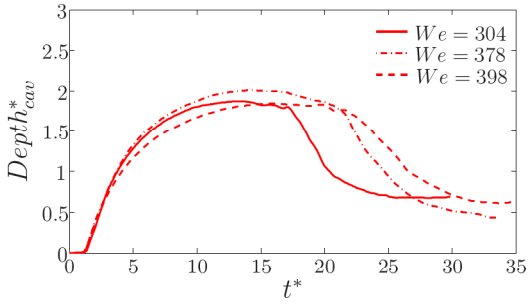

(c) Distilled water, $\varphi = 59°$

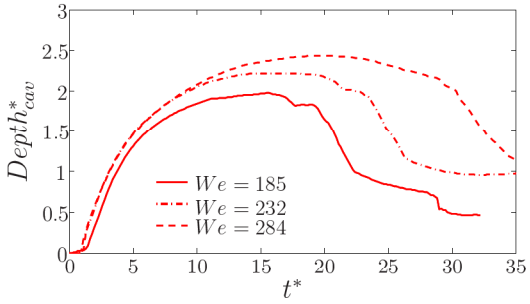

(d) Glycerine/water, $\varphi = 69°$

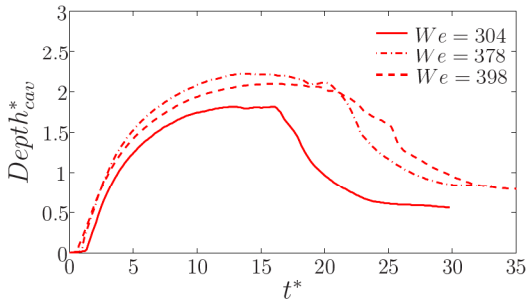

(e) Distilled water, $\varphi = 148°$

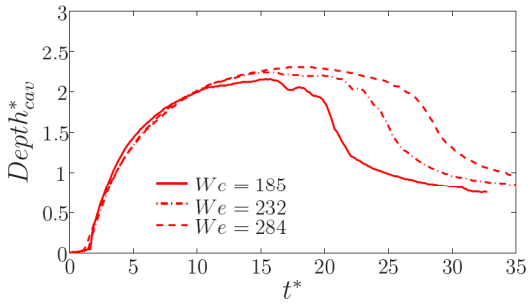

(f) Glycerine/water, $\varphi = 145°$

Figure 5.26: Evolution of the depth of the cavity in time as a function of the different Weber numbers for the impingement onto the small amplified wave. Comparison of the experimental results for different liquids and wave amplifications. For figure (a) and (b) the lines represent: lowest Weber number (solid lines), medium weber number (dashed lines) and highest Weber number (dotted lines)

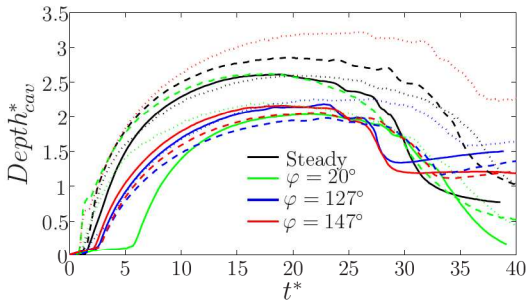

(a) Distilled water, large wave

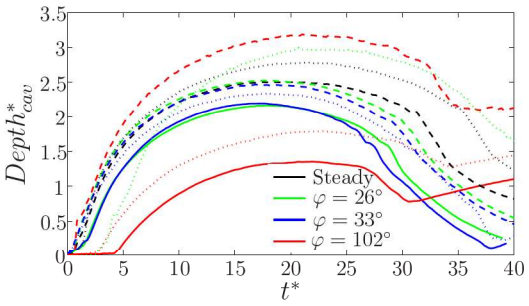

(b) Glycerine/water, large wave

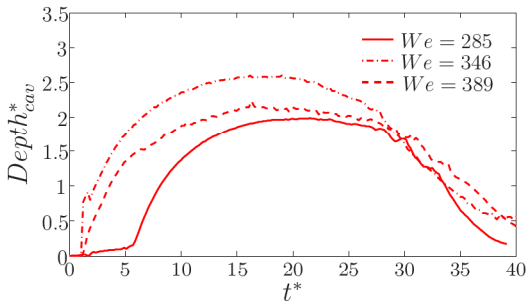

(c) Distilled water, $\varphi = 20°$

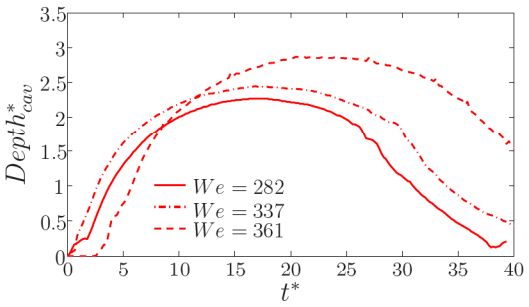

(d) Glycerine/water, $\varphi = 26°$

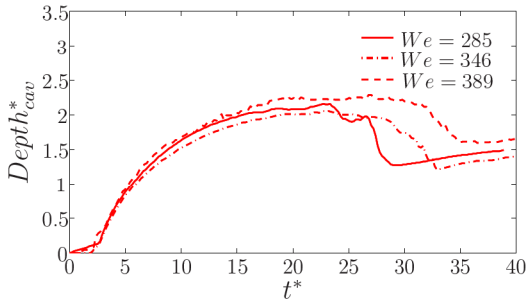

(e) Distilled water, $\varphi = 153°$

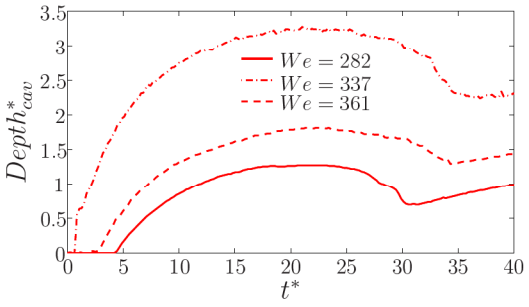

(f) Glycerine/water, $\varphi = 150°$

Figure 5.27: Evolution of the depth of the cavity in time as a function of the different Weber numbers for the impingement onto the large amplified wave. Comparison of the experimental results for different liquids and wave amplifications. For figure (a) and (b) the lines represent: lowest Weber number (solid lines), medium weber number (dashed lines) and highest Weber number (dotted lines)

reached depend in a distinct way on the Weber number of the impinging drop. In respectively Figure 5.28(a) and Figure 5.29(a) the maximum depth of the cavity and the times of maximum depth are shown as a function of the mean Weber number, measured over all the investigated phase angles of the wave.

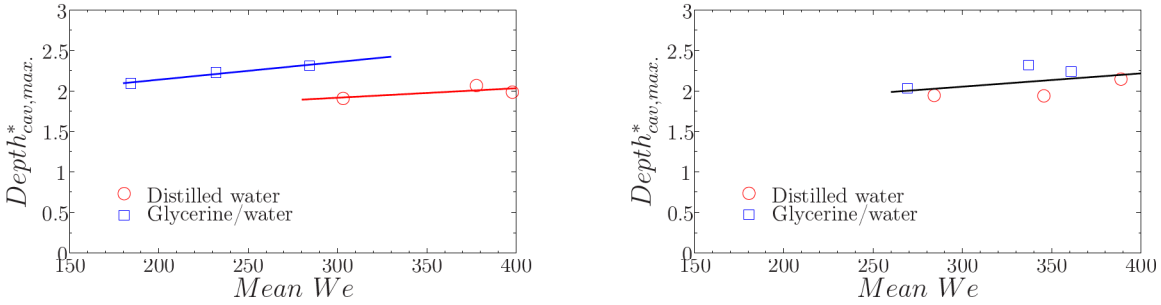

(a) Small wave (b) Large wave

Figure 5.28: Maximum depth of cavity as a function of the mean Weber number of the impinging drop for both wave amplifications

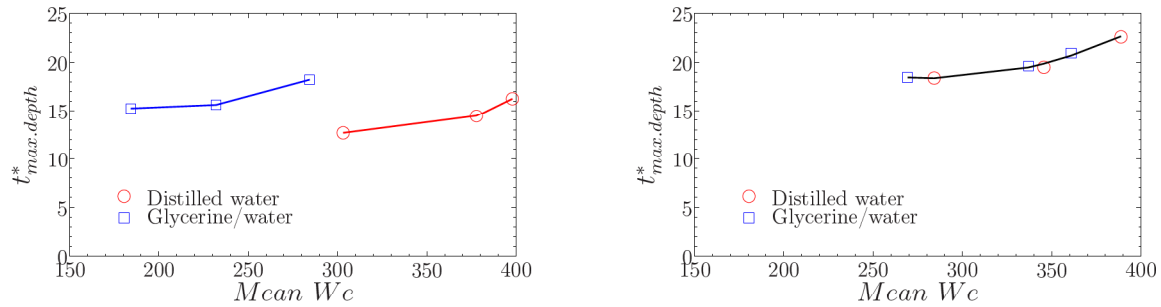

(a) Small wave (b) Large wave

Figure 5.29: Time to reach maximum depth of cavity as a function of the mean Weber number of the impinging drop for both wave amplifications

It is found that for both liquids a linear dependency of the maximum depth of the cavity on the mean Weber number is found, whereby for the same Weber number, the maximum depth for glycerine/water reaches a larger value than for distilled water. Due to the lower velocity of the solitary wave for glycerine/water, the horizontal component of the absolute velocity vector is smaller compared to distilled water. This means that for the same available kinetic energy upon impingement a larger amount is available to overcome the surface tension forces acting on the cavity. A smaller maximum amplitude of the wave leads to less interaction of the rim with the solitary wave. Therefore the rim can expand more and falls back onto the liquid surface at a later time instant, thereby merging with the liquid film and forming the capillary waves. A combination of these two factors results in a larger value of the maximum depth and a later time of maximum depth, as is observed in Figure 5.29(a). In this figure, it is noted that the time of maximum depth depends quadratically on the mean Weber number for both liquids. A larger mean Weber number leads to a later time instant at which the maximum depth of the cavity is reached, due to the higher value of the kinetic energy available at impingement and

the subsequent later time at which the surface tension forces can overcome the kinetic energy, which is in agreement with the impingement onto steady liquid films for increasing Weber numbers. It can therefore be concluded that for the small amplified wave the maximum depth and the time instant of maximum depth depend not only on the impingement velocity, but also on the viscosity of the liquid.

A later receding and subsequent retraction of the cavity is observed for both liquids for higher Weber numbers, due to the formation of a wider cavity, resulting in a large time-span during which the cavity recedes, hence a later retraction of the cavity. The results, presented in Figure 5.26(a) and 5.26(b), show only minor differences in the retraction of the cavities between the investigated wave-phases for the same Weber number.

The results for the depth evolution of the cavity in time for the impingements upon the large amplified solitary wave, presented in Figure 5.27(a) and 5.27(b), show for both liquids no clear dependency on the Weber number of the impinging drop. For both liquids the slopes of the curves do not correlate with the Weber number, but depend strongly on the phase of the wave upon impingement. For the impingement onto small wave-phases, below $\varphi \approx 40°$, or large phases, above $\varphi \approx 130°$, the interaction of the rim with the surface of the solitary wave is not significant, leading to a relatively small influence of the solitary wave on the cavity formation phase, as can be seen clearly by looking at the Shadowgraph images of the impingement process for $\varphi = 149$ (We = 293, distilled water) in the Figures 5.9 to 5.11, $\varphi = 147$ (We = 342, distilled water) and $\varphi = 144$ (We = 333, glycerine/water) in the Figures 5.12 to 5.14. For these wave-phases an approximately constant slope of the time change of the depth for all Weber numbers is found. For impingements onto a wave-phase in between these two regions, hence $40 \leq \varphi \leq 130$, a very distinct interaction of one of both sides of the rim with the surface wave is observed, thereby influencing both the expansion of the rim and the cavity.

In general a higher Weber number also leads for the large amplified wave in a higher value of the maximum depth and a later time instant at which this maximum depth is reached, although for the former variable the differences are smaller than for the smaller amplified wave, see Figure 5.28(b). In this figure it is noted that also for the larger amplified wave there exists a linear dependency of the maximum depth on the mean Weber number, but now the values for both liquids lie approximately on one curve. This means that the viscosity plays no role on the value of the maximum depth; the maximum depth is only a function of the terminal velocity of the drop upon impingement, since the values of the surface tension are approximately equal for both liquids. The same is observed for the time instant of maximum depth, Figure 5.29(b), where it is seen that the time instants depend quadratically on the Weber number, hence on the terminal velocity of the impinging drop squared.

A later receding and subsequent retraction of the cavity is observed for both liquids for higher Weber numbers, due to the formation of a wider and more inclined cavity, resulting in a large time-span during which the cavity recedes, hence a later retraction of the cavity. Large differences in the retraction of the cavities between the investigated wave-phases for the same Weber number are present for both liquids, because of the large influence of the phase of the wave upon impingement on the time change of the shape of the cavity.

The influence of the amplification of the solitary surface wave, hence its velocity and maximum amplitude, on the depth evolution in time is shown in Figure 5.30 for different phases of the wave upon impingement for glycerine/water.

In §(5.1.4) the observations were presented for the impingement of a distilled water drop onto the two different amplified solitary surface waves for the wave-phase $\varphi = 60°$ and $\varphi = 149°$.

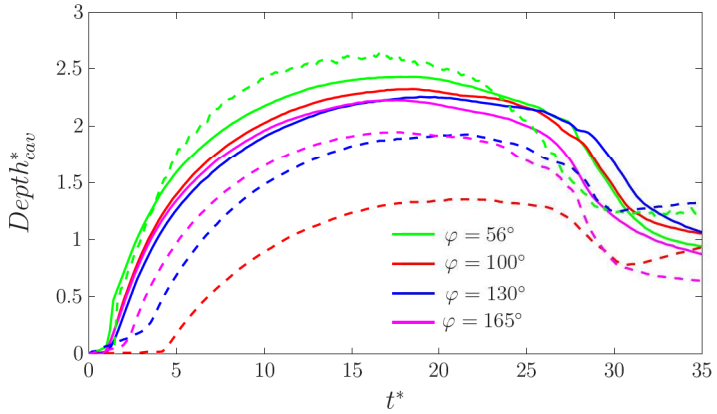

Figure 5.30: Evolution of the depth of the cavity in time for different wave amplifications. Comparison of the experimental results for the single drop impingement onto different phases of the small (solid lines, $We = 284$, $Fr = 316$ and $Re = 8,980$) and large (dashed lines, $We = 285$, $Fr = 296$ and $Re = 9,170$) wave for glycerine/water

With the use of these shadowgraph recordings it was seen that for the smaller wave-phase significant differences in the shape of the cavity are present for both solitary waves, the cavity for the larger amplified wave being much smaller in depth and diameter then for the smaller amplified wave. For $\varphi = 149°$, however, no large differences in the cavity were noted.

Comparing these observations with the results presented in Figure 5.30 for glycerine/water, it is seen that, with the exception of the results for $\varphi = 56°$, smaller depths are reached for the cavities upon impingement onto large amplified waves. Two factors are responsible for these differences between the two solitary waves. First of all, the more amplified wave has a larger value of the wave propagation velocity, due to which the horizontal component of the absolute velocity upon impingement is larger for this wave. This leads to a lower value of the kinetic energy, available for the radial expansion of the cavity. This explains the weaker slope of the curves for the large amplified wave in Figure 5.30.

Second, the impingement onto the large amplified solitary wave leads to a more distinct interaction of one side of the rim with this surface wave. Because of this interaction, a lower rim is formed at this side of the cavity, due to which at this side of the rim the gravity forces overcome the kinetic energy at an earlier time instant. The consequence is an earlier merging of the rim with the liquid surface and a subsequent earlier formation of the capillary wave at this side of the cavity. The cavity starts therefore its receding phase at this side of the cavity at an earlier time instant, leading to a lower maximum value of the depth of the cavity, as is observed in Figure 5.30. This difference in maximum depth of the cavity between both solitary waves becomes smaller for larger phases of the wave, because of a weaker interaction of the rim with the surface wave for higher phase angles. The time instants at which these maximum values are reached are approximately equal for both solitary surface waves, as can be seen clearly in Figure 5.29 for We ≈ 275.

The same differences between the two investigated surface waves is observed for the other investigated Weber numbers and phase-angles, which are not shown here, but an exception to this is the cavity formed upon impingement onto $\varphi = 56°$, Figure 5.30. Whereas for distilled water the impingement upon a wave-phase of $\varphi = 56°$ leads to a much smaller depth of the cavity for the larger amplified wave, see the Shadowgraph images of the impingement process

presented in the Figures 5.6 to 5.8, it is seen that for glycerine/water the time evolutions of the depth are approximately equal for both surface wave topologies at this wave angle. By looking at the shadowgraph recordings for glycerine/water, it is seen that the explanation can be found in the strong interaction of the corona with the leading edge of the solitary wave, leading to a very asymmetrical cavity, where the capillary wave at the left side of the cavity is formed almost immediately upon impingement. Because in the next time instants the cavity expands in radial direction and increases its inclination to the left, this left capillary wave increases in size and is directed downwards as a result of the increasing inclination of the cavity. At a certain time instant the absolute depth of the cavity is not described anymore by the cavity itself, but by this capillary wave, leading to a distinct difference in the time evolution of the depth of the cavity for this phase angle. Because the capillary wave at the left side is formed almost immediately after drop impingement, the receding and retraction of the cavity starts earlier, leading to an earlier time instant at which the maximum depth of the cavity is reached.

In Chapter 4 it has been shown that the properties of the liquid have a very distinct influence on the shape of the cavity, in particular on the time evolution of the depth and the diameter of the cavity. In this section the influence of the viscosity on the time evolution of the depth of the cavity will be discussed for both amplifications of the solitary wave. In Figure 5.31 the results are plotted for different phases of the wave upon impingement.

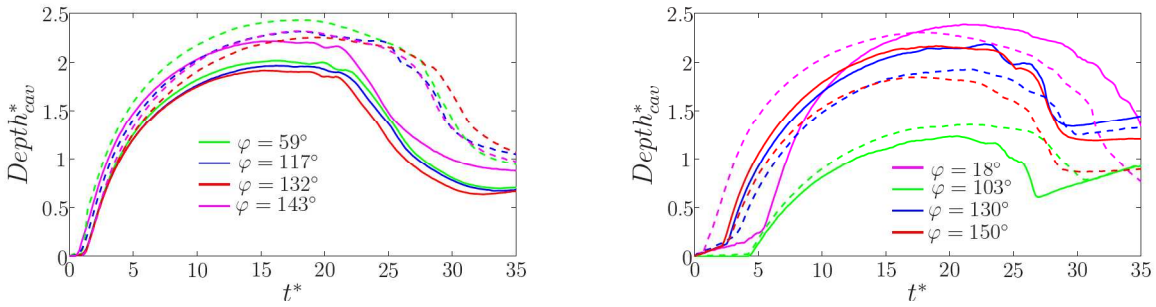

(a) Small wave

(b) Large wave

Figure 5.31: Evolution of the depth of the cavity in time for different liquids. Comparison of the experimental results for the single drop impingement onto different phases of the small wave (left) and large wave (right) for distilled water (solid lines) and glycerine/water (dashed lines). The impingement parameters are for the small wave $We = 398$ and $Re = 11,458$ (distilled water) and $We = 284$ and $Re = 8,980$ (glycerine/water) and for the large wave $We = 285$ and $Re = 9,170$ (distilled water) and $We = 282$ and $Re = 9,004$ (glycerine/water)

The differences in the time evolution of the depth of the cavity between the two liquids for the smaller wave are due to the larger velocity of the surface wave for distilled water. Due to this larger wave velocity, a larger horizontal absolute velocity component is present upon impingement, leading to less kinetic energy available for the expansion of the cavity. The surface tension forces, acting on the cavity and opposing the further expansion of the cavity, can therefore overcome earlier the kinetic energy, resulting in a smaller maximum cavity. This cavity has a lower value of its maximum depth, which is reached at an earlier time instant, than is found for glycerine/water. Because of the low values of the maximum amplitude of the solitary surface wave, only minor differences are observed between the various investigated phases of the wave. The faster conversion of the kinetic energy into surface tension energy and dissipated